Radioisotopic purity and imaging properties of cyclotron-produced ^{99m}Tc using direct ^{100}Mo(p,2n) reaction

N. M. Uzunov[1,71], L. Melendez-Alafort[12], M. Bello[2], G. Cicoria[5], F. Zagni[5], L. De Nardo[2,6], A. Selva[7], L. Mou[7], C. Rossi-Alvarez[7], G. Pupillo[7], G. Di Domenico[3], L. Uccelli[8], A. Boschi[8], F. Groppi[9], A. Salvini[10], A. Taibi[3], A. Duatti[11], P. Martini[2,7], M. Pasquali[3], M. Loriggiola[7], M. Marengo[5], L. Strada[13], S. Manenti[14], A. Rosato[4,12] and J. Esposito[7]

[1] *Faculty of Natural Sciences, Shumen University, Shumen, Bulgaria*
[2] *Department of Physics and Astronomy University of Padua, Padua, Italy*
[3] *Department of Physics and Earth Sciences, University of Ferrara and INFN Ferrara branch, Ferrara, Italy.*
[4] *Department of Surgery, Oncology and Gastroenterology University of Padua, Padua, Italy.*
[5] *Health Physics Service, Sant'Orsola-Malpighi Hospital, Bologna, Italy*
[6] *INFN, Sezione di Padova, Padova, Italy.*
[7] *INFN, Legnaro National Laboratories, Legnaro, (Padua), Italy.*
[8] *Department of Morfology Surgery and Experimental Medicine, Sec. of Imaging Diagnostic, University of Ferrara, Ferrara, Italy.*
[9] *Accelerator and Applied Superconductivity Laboratory and Department of Physics, University of Milan, Italy.*
[10] *Applied and Nuclear Energy Laboratory, University of Pavia, Pavia, Italy.*
[11] *Department of Chemical and Pharmaceutical Sciences, University of Ferrara, Ferrara, Italy.*
[12] *Veneto Institute of Oncology IOV – IRCCS, Padua, Italy*
[13] *Department of Chemistry University of Pavia, Pavia, Italy.*
[14] *INFN Milan branch, Milan, Italy.*

Abstract

Evaluation of the radioisotopic purity of technetium-99m (^{99m}Tc) produced at GBq amounts by proton bombardment of enriched molibdenum-100 (^{100}Mo) metallic targets at low proton energies (i.e. within 15–20 MeV), has been investigated. This energy range has been chosen since it is easily achievable by many conventional medical cyclotrons already available in the nuclear medicine departments of the hospitals. The main motivation for such a study is in the framework of the research activities at international level, conducted over the last few years to develop alternative production routes for the most widespread radioisotope used in medical imaging. The analysis of technetium isotopes and isomeric states (^{9x}Tc) present in the pertechnetate saline Na^{99m}TcO$_4$ solutions, obtained after the extraction/purification procedure, reveals radionuclidic purity levels in compliance with the limits recently issued by (European Pharmacopoeia, 9.3, 2018). Moreover, the impact of ^{9x}Tc contaminant nuclides on the final image quality has been thoroughly evaluated analyzing the emitted high-energy gamma rays and their influence on the image quality. The spatial resolution of images from cyclotron-produced ^{99m}Tc acquired with a mini gamma camera was determined and compared with that obtained using technetium-99m solutions eluted from standard ^{99}Mo/^{99m}Tc generators. The effect of the increased image background contribution, due to Compton-scattered higher-energy gamma rays (E_γ > 200 keV), which could cause image contrast deterioration, was also studied. It is concluded that, due to the high radionuclidic purity of cyclotron-produced ^{99m}Tc using ^{100}Mo(p,2n)^{99m}Tc reaction at a proton beam energy in the range 15.7– 19.4 MeV, the resulting image properties are well comparable with those from the generator-eluted ^{99m}Tc.

[1] Corresponding author.
Permanent address: 115 Universitetska str., Faculty of Natural Sciences, University of Shumen, 9712 Shumen, Bulgaria
E-mail addresses: nikolay.uzunov@lnl.infn.it; n.uzunov@shu.bg (Nikolay Mihaylov Uzunov)

Keywords: radionuclidic purity, radioisotopic purity, image spatial resolution, Compton scattering, image contrast, European Pharmacopoeia.

INTRODUCTION

Technetium-99m (^{99m}Tc), a metastable nuclear isomer of technetium-99 (^{99}Tc), is still the most used radionuclide for diagnostic imaging procedures in nuclear medicine. More than 80% of all the morphological and dynamic organ and total-body diagnostic imaging is performed using ^{99m}Tc-labelled pharmaceuticals. Because of its well-known chemical properties, it can be easily bound to different types of pharmaceutical products (Arano 2002, Banerjee et al. 2001, Banerjee et al. 2005, Boschi et al. 2012, Boschi et al. 2013). In addition, the radionuclide has almost ideal nuclear properties such as a short half-life ($T_{1/2}$=6.0067±0.0005 hrs, 1σ (Browne et al., 2017) and is the perfect low-energy monoenergetic gamma-ray emitter (Eγ = 140.5 keV (89%)) for imaging (Eckelman 2008, Ott et al. 1988).

Technetium-99m is usually available in portable ^{99}Mo/^{99m}Tc generators (IAEA 2013, Vučina 2001), where it is generated by a β^- decay of ^{99}Mo parent nuclide. The alumina column inside the generator is pre-adsorbed with ^{99}Mo ($t_{1/2}$ = 65.98 h), produced in nuclear reactors as Fission Product (FP) of Highly Enriched Uranium, Weapon-Grade (HEU-WG) material (^{235}U enrichment > 80wt %). For decades such a supply system ensured a widespread distribution of ^{99m}Tc radionuclide at the end-users' location, even far from the manufacturing center.

Nowadays the majority of the world's large- and medium-scale routine production is carried out mainly at five major ageing research reactors, most of them commissioned more than 50 years ago (Dodd 2002, Krijger 2013). Due to unexpected outages or planned reactor shutdowns, significant ^{99m}Tc shortages on the international market have already occurred in recent years (2009/2010). This fact, along with the forthcoming permanent shutdown planned for some of the reactors concerned, has prompted at global scale the search for alternative non-HEU-based ^{99m}Tc production routes (IAEA 2013, Dodd et al. 2002, Krijger et al. 2013, NEA 2017).

Since the long-term future of nuclear medicine is foreseen with a larger demand for ^{99m}Tc, mid-term and short-term solutions are to be taken into consideration as well (IAEA 2013). Following the new trends for non-HEU-based radionuclides production methods, the research activities at the Legnaro National Laboratories (LNL) of the Italian National Institute for Nuclear Physics (INFN) were oriented towards alternative, cyclotron-driven routes. These activities became later a part of a large international collaborative effort under a Coordinated Research Project (CRP) framework, launched on the same matter by IAEA in 2011, results of which have been recently issued (IAEA 2017).

The research program carried out so far aimed at determining, from a comprehensive theoretical point of view, the best irradiation conditions (Esposito et al. 2013) for direct production of cyclotron-produced ^{99m}Tc, referred to as "cyclotron-^{99m}Tc". A general agreement was found with the unique other similar study published earlier (Celler et al. 2011). The article is however based on a different theoretical approach and uses some limiting/simplifying criteria to reduce the amount of data (e.g. ignoring reaction routes with excitation function lower than 1 mb; isotopes/isomeric states with $T_{1/2} \leq 5$ min considered as directly producing daughters nuclides, etc.). This resulted in an incomplete/warped mapping of all possible reaction routes and decay chains leading to ^{9x}Tc nuclide yields. In addition, the post End of Bombardment (EOB) time evolution of the radionuclidic purity (RNP) is anyway missing. Moreover, the experimental results produced (Uccelli et al. 2013, Manenti et. al., 2014, Pupillo et al., 2014, Pupillo et al., 2015) confirmed that a very worthwhile approach for ^{99m}Tc production, *via* the ^{100}Mo(p,2n) reaction route, through proton bombardment on

highly ^{100}Mo-enriched molybdenum metallic targets, might be feasible. Such results were confirmed at international level by other research groups (IAEA 2017). Actually, both theoretical and experimental data have convincingly shown that the optimal proton beam energy assuring a ^{99m}Tc supply in as large as enough amounts for clinical applications, having radionuclidic purity levels comparable to the generator-^{99m}Tc, falls in the range 15 – 20 MeV. According to current predictions (NEA, 2017), the increasing ^{99m}Tc world demand for medical applications will outpace the supply options in the nearest future, if all of the additional conventional irradiation and processing capacity planned to be put into operation in the next coming years are not fully realized. Therefore, it is worth searching for opportunities to exploit the number of medium/low-energy and low-current conventional medical cyclotrons, already available in the large hospital centers, which could meet the routine local demand. It should be pointed out that such a motivation about the in-house approach to the cyclotron production of ^{99m}Tc is exactly opposite to the one envisioning a few centralized medical isotope production centers. The latter is based on unconventional high-current cyclotrons capable to ensure a daily production to meet the clinical demand of a large metropolitan area (Ruth, 2009, 2014, Pillai et al., 2013, Bénard et al., 2014). In this respect, the main research line currently running at LNL INFN is focused on the R&D of an easy-to-use technology for a future local supply of cyclotron-^{99m}Tc for a traditional radionuclide production in the hospitals, based on the available medical cyclotron's network in Italy.

Along with the optimal physical parameters to effectively have a cyclotron-^{99m}Tc production, a concern is anyway the yield of other ^{9x}Tc-contaminant nuclides originating from (p,xn) reactions routes on the other ^{9x}Mo isotopes in the ^{100}Mo-enriched target material (Celler et al. 2011, Lebeda et al. 2012, Esposito et al. 2013, Selivanova et al. 2015). The presence of gamma- and beta- emitters having higher energy spectra will thus result in image quality degradation, with respect to the standard generator-^{99m}Tc. Therefore, to meet the issue whether the best experimental conditions for the alternative ^{99m}Tc production route may be obtained by using the already available hospital cyclotrons, a series of proton-beam irradiation experiments in the energy range 16–19 MeV were conducted. In all our tests, we used a slightly downgraded but still highly ^{100}Mo-enriched molybdenum target material. The main goal was to determine quantitatively the influence of the beam irradiation parameters on the final image quality metrics. The results from the experiments allowed us to optimize the production conditions (target composition, beam irradiation conditions, extraction procedure, etc.) based on the quality of the resulting gamma-ray images, and to establish acceptable limits (exploitation time intervals such as minimum and maximum time intervals after EOB), for its use in diagnostic clinical procedures. The results of the series of gamma-ray spectroscopy measurements and image quality tests, performed on the final pertechnetate solution [^{99m}Tc][TcO_4]$^-$ after dissolution and separation/purification of the proton-irradiated ^{100}Mo-enriched molybdenum targets, are herewith discussed.

MATERIALS AND METHODS

Target preparation and irradiation

In all performed irradiation tests we used thin, square-shaped, metal foils from ^{100}Mo-enriched molybdenum material, stacked together and installed in a copper target holder with a central hole on the beam-facing side. No energy degradation has occurred prior the stacked-foils targets were hit at the chosen beam energies, shown in Table 1. The target mass thicknesses in these irradiations were smaller than the optimal ones for cyclotron-Tc production at the reported energies, i.e. ~600

mg/cm^2 for the irradiation at 19.2 MeV and ~290 mg/cm^2 at 15.7 MeV, thus covering thus the useful range (19.2– ~9.6) MeV and (15.7– ~9.6) MeV respectively as reported in (Esposito et al. 2013). The goal of these tests was to obtain amounts of cyclotron-Tc enough for further gamma spectrometry measurements and for the imaging experimental tests. For each run, 5-6 molybdenum metal foils (~1.1-1.2 cm side length) with total mass thicknesses as reported in Table 1, were routinely produced at the LNL target laboratory. They were prepared by lamination process technique from enriched molybdenum metal powder, melted under temperature-controlled conditions in argon gas atmosphere. The isotopic composition of the enriched molybdenum material used in this study was a good compromise between the largest and smallest ^{100}Mo-enrichment levels available on the market: ^{100}Mo (99.05%), ^{98}Mo (0.54%), ^{97}Mo (0.07%), ^{96}Mo (0.11%), ^{95}Mo(0.10%), ^{94}Mo (0.05%), and ^{92}Mo (0.08%). It was purchased from the ISOFLEX company (ISOFLEX Batch, 2012).

Irradiations of ^{100}Mo-enriched staked-foils targets with proton beams were carried out on two different facilities. The first two runs were at 19.2 MeV energy at the EU Joint Research Centre (MC-40 Scanditronix Cyclotron, JRC Laboratory, Ispra, Italy). Other two proton irradiation experiments at lower energy (15.7 MeV) were instead carried out at the General Electric (GE), model PETtrace 16-9, medical cyclotron, located at St. Orsola-Malpighi Hospital, Nuclear Medicine Department (Bologna, Italy). After each irradiation, the ^{100}Mo-enriched foils of the stacked targets underwent the same chemical dissolution/separation/purification process, as recalled in the next section. The obtained liquid samples of ^{9x}Tc-pertechnetate ($^{9x}TcO_4^-$) were labelled as "TC-TEST_X", where X denotes the number of the irradiation experiment as reported in Table 2. The asymmetric overall uncertainties reported in Table 1, about the In-target activity estimation at EOB of tests conducted at the MC-40 cyclotron only, are due to the imperfect accommodation of target holder during bombardments, causing a slight misalignment with respect to beam axis. This aspect (well known by cyclotron operators) was obviously taken into account to correct the current integrator data recorded. The activity uncertainties reported in Table 2 are instead the measurement uncertainties of the dose calibrators (DC) used.

Table 1. Main stack-foils target data for the irradiation experiments.

Test ID	Cyclotron	Beam energy [MeV]	Beam current [μA]	Target mass thickness [mg·cm^{-2}]	Irradiation time [min]	In-target ^{99m}Tc activity at EOB [GBq]
TC-TEST_1	MC-40	19.2±0.5	25	146.5±7.2	70	$3.80^{+0.4}_{-0.9}$
TC-TEST_2	MC-40	19.4±0.6	25	144.7±7.1	80	$4.10^{+0.4}_{-0.9}$
TC-TEST_3	PET-Trace	15.7±0.4	20	119.6±5.8	90	3.60 ± 0.18
TC-TEST_4	PET-Trace	15.7±0.4	10	121.5±5.9	62	1.17 ± 0.06

Table 2. Details of different cyclotron-^{99m}Tc samples prepared for additional analyses.

Test ID	Original sample	Aliquot volume	Dilution	New Aliquot	Place	Activity	Destination
TC-TEST_1A	TC-TEST_1	10 μl	No	---	Small Eppendorf vial	25.72 kBq ±5%	Spectrometry analyses
TC-TEST_2A	TC-TEST_2	7 ml	Yes (7ml MilliQ water)	---	vial	163.91 MBq ±5%	Imaging analyses
TC-TEST_3A	TC-TEST_3	36 μl	Yes (964 μl water).	10 μl	Small Eppendorf vial	27.75 kBq ±5%	Spectrometry analyses
TC-	TC-	10 μl	No	---	Small	30.34 kBq	Spectrometry

TEST_4A	TEST_4				Eppendorf vial	±5%	analyses
TC-TEST_4B	TC-TEST_4	1.23 ml	Yes (5 ml water)	---	vial	3.73 MBq ±5%	Imaging analyses

Samples processing and ^{9x}Tc extraction and purification procedure

The extraction and purification of cyclotron-^{99m}Tc from irradiated targets was performed using the optimized, fully automated, remotely controlled module, specifically developed and set up by our group for cyclotron-^{99m}Tc production at GBq quantities. The module is based on the solvent extraction method using Methyl Ethyl Ketone (MEK) (Martini et al. 2016) and was realized in collaboration with the Nuclear Medicine department group of St. Orsola Hospital in Bologna (Martini et. al 2013). It proceeds in four-step stage: (i) molybdenum foils dissolution in a hot hydrogen peroxide (H_2O_2) plus sodium hydroxide (NaOH) solution; (ii) solvent extraction of ^{9x}Tc-pertechnetate ($^{9x}TcO_4^-$) into the MEK organic phase; (iii) purification of the extracted ^{9x}Tc-pertechnetate through chromatographic columns; (iv) collection of ^{9x}Tc under $Na^{9x}TcO_4$ form by alumina columns elution with a physiological solution. Details about the procedures followed, as well as the determination of all chemical QC parameters in the final ^{99m}Tc product with respect to the (European Pharmacopoeia, 9.3, 2018) can be found in (Martini et al., 2016).

Samples with low activities, suitable to perform gamma spectrometry analyses, were then prepared as shown in Table 2 from the aforementioned TC-TEST_X solutions by further diluting. The aliquot volume of samples TC-TEST_1A, TC-TEST_3A and TC-TEST_4A was 10 µl. Samples TC-TEST_2A/4B, having a much higher activity, were used for imaging analyses. However, a vial with an aliquot taken from sample TC-TEST_4B has been used for spectrometry analyses as well. It was placed in a 6 mm thick lead container to suppress the intense 140 keV emission from ^{99m}Tc for the gamma-ray spectroscopy measurements of the higher-energy gamma rays of the other technetium isotopes.

Gamma-ray spectrometry analysis setup

All gamma-ray spectrometry measurements were carried out using the high-sensitivity, low-background setup of the LNL Geophysics Laboratory as reported by (Xhixha et al. 2013). The spectrometry setup consisted of a lead/copper shielded compartment with two opposite germanium semiconductor detectors facing each other 5 cm apart and a system for positioning the measured samples in between. The shielding covered both detector heads and their rear parts, thus reducing the background radiation in the gamma spectra by two orders of magnitude. For our measurements we used high-volume HPGe gamma-ray detectors with larger detector volumes than the ones described in (Xhixha et al. 2013), with 80% relative efficiency and energy resolution of 2.1 keV at 1332.5 KeV. Detectors' outputs were connected to 7611/L Silena spectroscopy amplifiers, attached to an EtherNIM 919E Ametek ADC converter. The ADC converter was controlled by Maestro 32 software. The acquired gamma ray spectra were analyzed using ANGES software (IAEA 2002).

Both detectors of the system could be used in a single mode when spectra acquisitions were made using a single detector, as it was proceeded with the activity measurements of TC-TEST_1A, TC-TEST_3A and TC-TEST_4A samples. More elaborated spectra acquisitions could be performed in tandem mode, when the acquisition is performed simultaneously by both detectors and then a unique gamma-ray spectrum is created by summation of the counts of the two simultaneously measured spectra, after a rebinning procedure (Xhixha et al. 2013). While the energy calibration in tandem mode is performed on both detectors independently, the efficiency calibration and the gamma-ray spectra analyses are performed using the common spectra after the summation. The larger solid angle covered by both detectors is close to 4π. It improves the limits of detection,

enhances the precision of the measured activities and reduces the systematic error, caused by not precise sample-to-detector positioning. As it turned out, this mode was very useful for the detection and analysis of lower-activity technetium nuclides and we applied it for the analysis of sample TC-TEST_4B.

A sample holder positioned the samples at a distance of 25 mm from each germanium detector. The efficiency calibration of the semiconductor detectors was carried out in the range 60 keV − 1700 keV by using certified point-like calibration sources ^{152}Eu, ^{57}Co and ^{241}Am (Eckert & Ziegler, Nuclitec GmbH, Germany). The calibration was performed according to the IEC 61452 standard, and has been routinely verified before the experiments. Similar efficiency calibration procedure with the same point-like calibration sources was used for TC-TEST_4B sample. Since the sample was to be measured also in a lead container, the efficiency calibration was performed also by placing the point-like gamma-ray calibration sources in the same lead container. Our preliminary tests for this geometry demonstrated that the deviations of the measured activities with the lead shielding were less than 5%.

The activities of samples TC-TEST_1A, TC-TEST_3A and TC-TEST_4A were very low and the liquid volumes inside small enough to be considered as point-like sources. Due to the time span needed for target chemistry procedures and the samples delivery to the LNL Geophysics Laboratory, the first gamma spectra have been collected 8 hours after the EOB for TC-TEST_1 sample. That was because of the Ispra – Ferrara – Legnaro route, while for the remaining TC-TEST_X samples the delay time shortened to 6 hours (Ferrara – Legnaro route). The activities for short-half-life nuclides (i.e. those having life-times shorter than ~6 hours) ^{93g}Tc, ^{93m}Tc, ^{94g}Tc, ^{94m}Tc and ^{99m}Tc in the samples TC-TEST_1A, TC-TEST_3A and TC-TEST_4A were determined from several spectra acquisitions with duration of 20 minutes each. The activities of technetium isotopes with medium-half-life (i.e. a few days), such as ^{95g}Tc, were measured 48 hours later, for acquisition times of 4 hours. Finally, the activities of the longer-lived isotopes (i.e. ^{95m}Tc, ^{96g}Tc and ^{97m}Tc) were measured 8 days later for acquisition times of 6 hours. All the measured activity concentrations were then calculated back to the target beam stop (EOB) event. Presence of the other short-lived isomer state, ^{96m}Tc was difficult to detect inside our samples, taking into account both the irradiation parameters/delivery time, and the low gamma-ray energy for IT transition and very low absolute gamma-ray intensity. A list of the most-commonly present Tc-isotopes in cyclotron-Tc with their respective half-lives and main gamma emissions are reported in Table 3.

Table 3. Summary of main nuclear decay data for commonly produced cyclotron-^{9x}Tc radionuclides (source NNDC online database**)**

Nuclide	$T_{1/2}$	Decay mode	Main gamma lines	
			Eγ [keV]	Iγ [%]
^{99m}Tc	6.0072 h	IT (99.9963%)	140.511	89
			142.63	0.0222
		β^- (0.0037%)	89.6	0.001
^{93m}Tc	43.5 m	IT (77.40 %)	391.83	58.3
		EC (22.60%)	2644.58	14.3
^{93g}Tc	2.75 h	EC (100.00 %)	1362.94	66.2
			1520.28	24.4
^{94m}Tc	52.0 m	EC (100.00 %)	871.05	94.2
			1868.68	5.7
^{94g}Tc	293 m	EC (100.00 %)	702.64	99.6
			871.05	99.9

^{95m}Tc	61 d	EC (96.12 %)	204.117	63.2
			582.082	30.0
		IT (3.88 %)	38.9	7.5E-5
^{95g}Tc	20.0 h	EC (100.00 %)	765.789	93.8
			1073.71	3.74
^{96m}Tc	51.5 m	IT (98.00 %)	34.2	0.0259
		EC (2.00 %)	778.22	1.9
			1200.15	1.1
^{96g}Tc	4.28 d	EC (100.00 %)	778.22	99.76
			849.86	97.56
			812.54	82.0
^{97m}Tc	91 d	IT (96.06 %)	96.5	0.32
		EC (3.94 %)	--	--

Time evolution activity curves for all technetium isotopes were obtained from the gamma-ray spectra of TC-TEST_4B sample, placing the vial with and without the 6 mm thick lead shielding. The first tandem-mode acquisition (sample inside Pb container) aimed at detecting the short lifetime radionuclides. It started 7 hours after EOB and lasted 24 hours. The second tandem-mode run (without lead shielding) began right after the first one and the acquisition continued about 100 hours. The system automatically saved every hour the gamma-ray spectra in both runs for further processing. Time evolution curves of the activity concentration for ^{99m}Tc and the other ^{9x}Tc contaminant nuclides were obtained by data fit procedures applied on each spectrum. The activity concentrations were then rescaled back to the EOB time.

Imaging resolution performance experimental setup

One of the main issues to be investigated was to estimate the influence of the other ^{9x}Tc contaminant isotopes of the cyclotron-^{99m}Tc on the imaging parameters, comparing them to the corresponding ones of the reference source from generator-^{99m}Tc. Most of the technetium contaminant isotopes yield gamma rays with energies high enough to penetrate the septa of the gamma camera parallel-holes collimators; they can scatter there or furthermore backscatter from the scintillator itself or from the gamma camera backing and pass through the energy filter. Moreover, a great part of these isotopes are nuclei having excess of protons and usually emits EC/β+ particles with energies of several hundred keV (e.g. ^{95g}Tc double β+ spectrum, (1) <Eβ+> =225.8 keV, Endpoint energy 1528 keV, and (2) <Eβ+> =336.8 keV, Endpoint energy 1732 keV (Basu, et al 2010)), see also National Nuclear Data Center (NNDC) online database (www.nndc.bnl.gov/). The annihilation of the positrons in the matter creates peak at 511 keV with a corresponding lower energy Compton region superimposed on the gamma-ray spectrum region around 140 keV. These possible processes give rise to doubts that the presence of ^{9x}Tc isotopes in the solutions could increase the image background and worsen the spatial resolution of the imaging detectors.

To assess the differences in the image quality that could be expected in the images from cyclotron-^{99m}Tc, compared to that from a standard generator-^{99m}Tc, a series of spatial resolution measurements were carried out by using a mini gamma camera for scintimammography applications. The mini gamma camera Mammocam 1000 (Preciosa Crytur, Turnov, Czech Republic) consists of a segmented CsI(Tl) scintillator, optically coupled to R3292 Hamamatsu

photomultiplier. The parallel-hole lead collimator had a thickness of 35 mm and 1.7 mm hexagonal holes with septa of 0.2 mm. The camera had a circular field of view having a diameter of 90 mm.

As shown in Figure 1, an experimental setup, made of ten parallel capillary tubes with a gap distance of 10 mm each was prepared for continuous imaging investigations by using different ^{99m}Tc-pertechnetate solutions. The capillary tubes, connected in series through flexible tubes, were linked to a circuit comprising small reservoir and a peristaltic pump, ensuring a constant liquid flow inside the system. Such a system was designed since we were to maintain a certain count rate in the beginning of each image acquisition without changing the geometry of the experiment (the capillary tubes position with respect to the gamma camera and the camera-to-object distance). This was achieved by addition in the reservoir of more concentrated solution of the studied ^{99m}Tc pertechnetate at the beginning of each image acquisition. In addition, the complete change of the liquid was easily done by emptying the reservoir and refilling it with the next solution. Furthermore, the constant liquid flux in the capillary tubes prevented the formation of air bubbles in the capillary tubes during the long-term image acquisitions. The distance between the capillary tubes and the top of the gamma camera was set at 12 mm. Such a distance has been chosen as a compromise between the image acquisition time and the minimum number of counts in the image profile. The preliminary analysis demonstrated that the image acquisition time had to be shorter than the half-life of ^{99m}Tc so as to detect observable image changes. However, it had to be long enough to collect sufficient count statistics in order to carry out reasonably good profile fits. Taking into account the activity levels of the technetium solutions we had, we could go down to acquisition times within the interval of 90 – 180 minutes at the given distance.

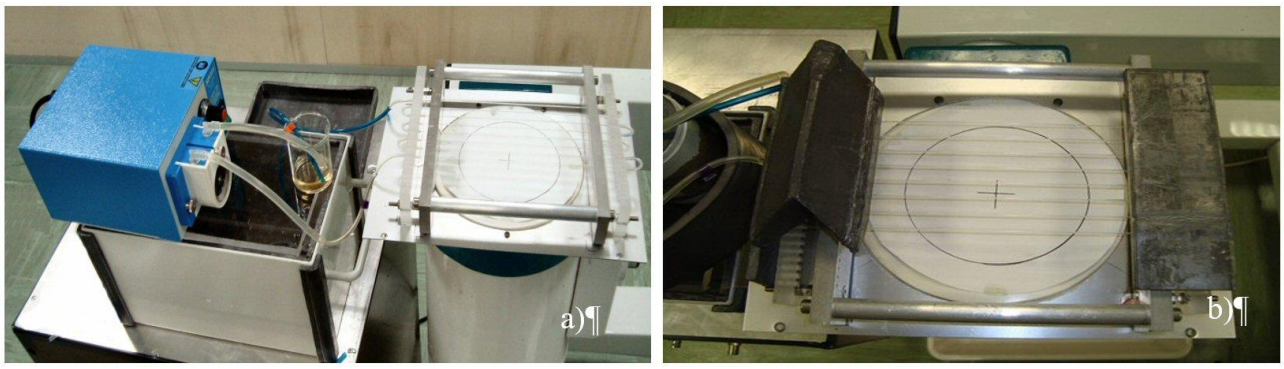

Fig. 1. The experimental setup for imaging resolution studies: (a) the system with parallel capillary tubes containing ^{99m,g}Tc solutions, the peristaltic pump and the gamma camera beneath the capillary tube system; (b) gamma camera top view with capillary tube system and the lead shielding during an image acquisition.

The imaging performance of the gamma camera was assessed by analyzing the images of the capillary system filled with circulating solutions. The overall camera spatial resolution was then calculated as the averaged full width at half maximum (FWHM) of the line spread function (LSF), calculated from the line profiles perpendicular to the capillary tubes using the deconvolution procedure reported in (Uzunov et al. 2004, Uzunov et al. 2005).

Gamma-ray background measurement system

A review conducted on the most intense (i.e. larger than 60%) gamma-ray emissions from ^{9x}Tc isotopes present in the cyclotron-^{99m}Tc pertechnetate solution, reveals that the gamma rays with energies higher than 140 keV cover a relatively large interval, from 204.1 keV (^{95m}Tc) up to

1363.02 keV (^{93g}Tc). Figure 2 shows the energy of Compton scattered gamma rays, emitted in this energy interval as a function of the scattering angle. The energy window of the imaging detectors for ^{99m}Tc such as gamma cameras, is usually set in 15% narrow interval around the peak of ^{99m}Tc (E_γ = 140 keV), shown in grey on figure 2. This window is far below the energies of the emitted gamma rays of the ^{9x}Tc isotopes in the solution. However, from the figure is seen that it is achievable by the great part of the gamma rays undergone large-angle Compton scattering in the matter (tissues) as well as of the backscattered highest gamma-ray energies after a few consequent multiple forward Compton scattering. A consequence of such large-angle Compton scattering of higher-energies gamma rays could be the increase of the background in the images and could result in a degradation of both the image contrast and spatial resolution. Another possible background contribution could originate from the higher-energy gamma rays crossed directly the collimator septa and undergone Compton backscattering in the camera back-compartment and then registered by the scintillator. However, while the problem of the background in this case is solved by an appropriate choice of high-energy gamma-ray collimators, the effect of the increased background resulting from the scattering in the medium cannot be eliminated by the hardware. In this article we pay special attention to the contribution of the scattering in the medium only.

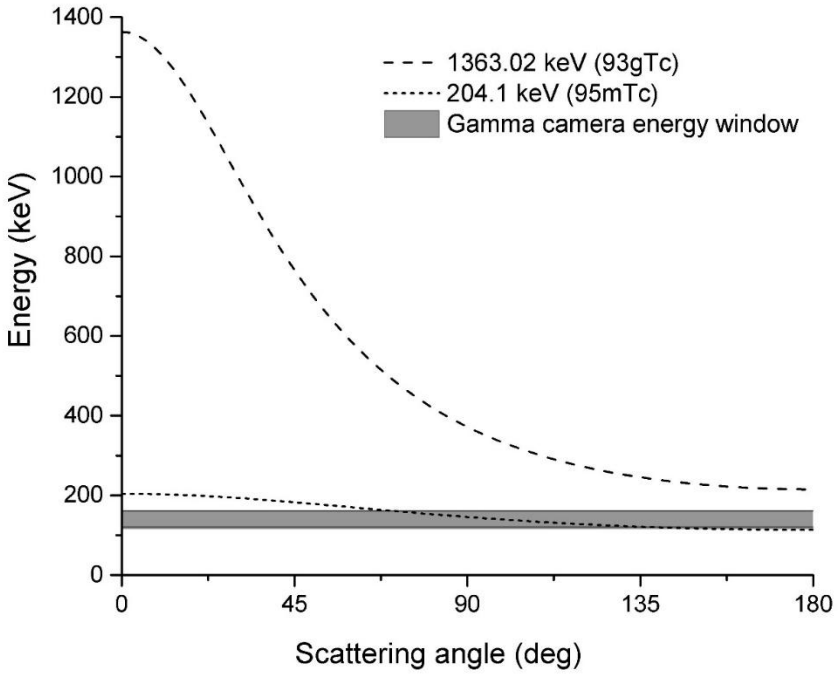

Fig. 2. Angular energy dependence of Compton-scattered gamma rays calculated for the ^{9x}Tc isotopes with the lowest (204.1 keV) and the highest (1363.2 keV) energy emission. The gamma camera energy window is indicated in grey color. Adapted from "A Study on the Gamma-Ray Background of the Images Obtained Using Accelerator-Produced ^{99m}Tc" by Uzunov et al., 2015, LNL Annual Report, p. 152. Copyright 2015 by the LNL Annual Report. Adapted with permission.

To determine the influence of the Compton-scattered higher energy gamma rays from cyclotron-^{9x}Tc contaminant nuclides on the image quality, a simple experimental setup was designed. It is based on a set of three parallel capillary tubes filled with a circulating ^{99m}Tc solution. A layout of the experimental setup is shown in figure 3(a), whereas a schematic sketch of the system, including

a mini gamma camera underneath is shown in figure 3(b). Capillary tubes, denoted as T_1, T_2 and T_3, are fixed on a support frame at different distances from the bottom. The device is then fully immersed in a water tank and placed above the mini gamma camera. The goal was to simulate the scattering in the soft tissues and its contribution to the image background. The water level inside the tank was chosen to be slightly above the highest capillary tube. The amount of back-scattered gamma rays and those scattered at larger angles in water is thus expected to be larger around the capillary tube zone closest to the detector (Figure 3(b)). According to the Klein-Nishina formula (Klein and Nishina 1929), Compton scattering is possible at large scattering angles and the backscattering can be observed for gamma-ray energies in the region of 200 keV to 1400 keV. The expected image profile would result in three peaks rising from a linearly decreasing background as it is schematically shown in Figure 4.

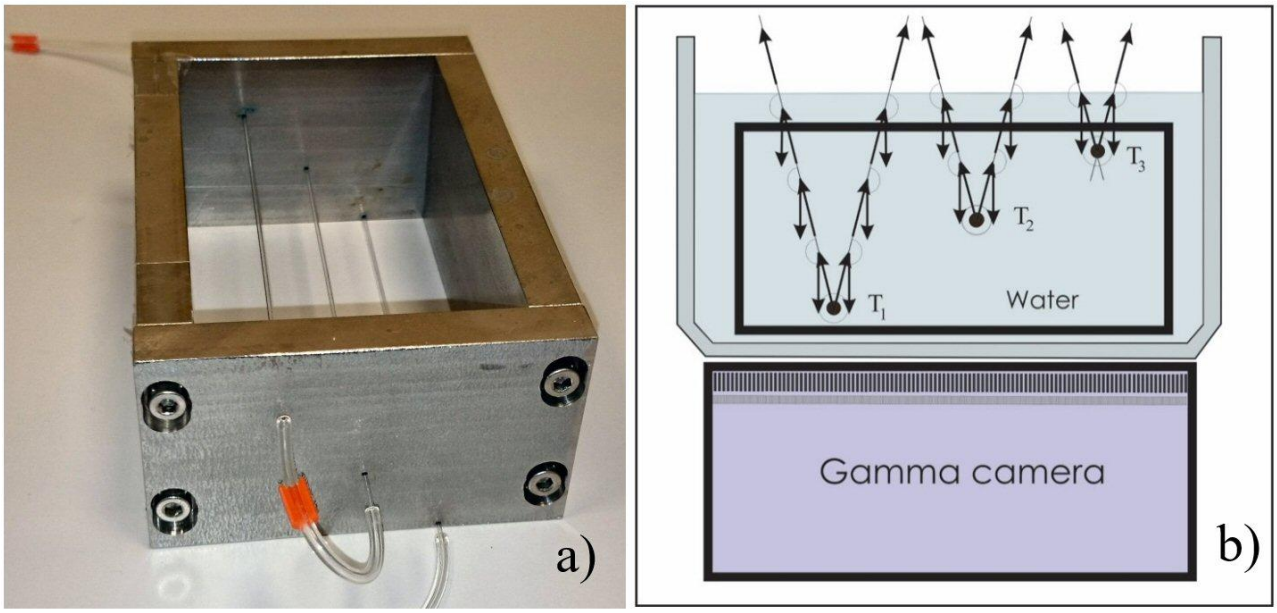

Fig. 3. Setup for Compton scattering background assessment experiment (a). Schematic sketch of the experimental setup with three capillary tubes, at different height positions indicated as T_1, T_2, and T_3, and the gamma camera below (b). The upward arrows show directions of the emitted gamma rays from capillary tubes opposite the collimator and gamma camera, while the downward arrows point out the backward Compton-scattered ones. The larger the water layer thickness above capillary tubes, the higher the Compton-backscattered gamma contribution expected. Adapted from "A Study on the Gamma-Ray Background of the Images Obtained Using Accelerator-Produced ^{99m}Tc" by Uzunov et al., 2015, LNL Annual Report, p. 152. Copyright 2015 by the LNL Annual Report. Adapted with permission.

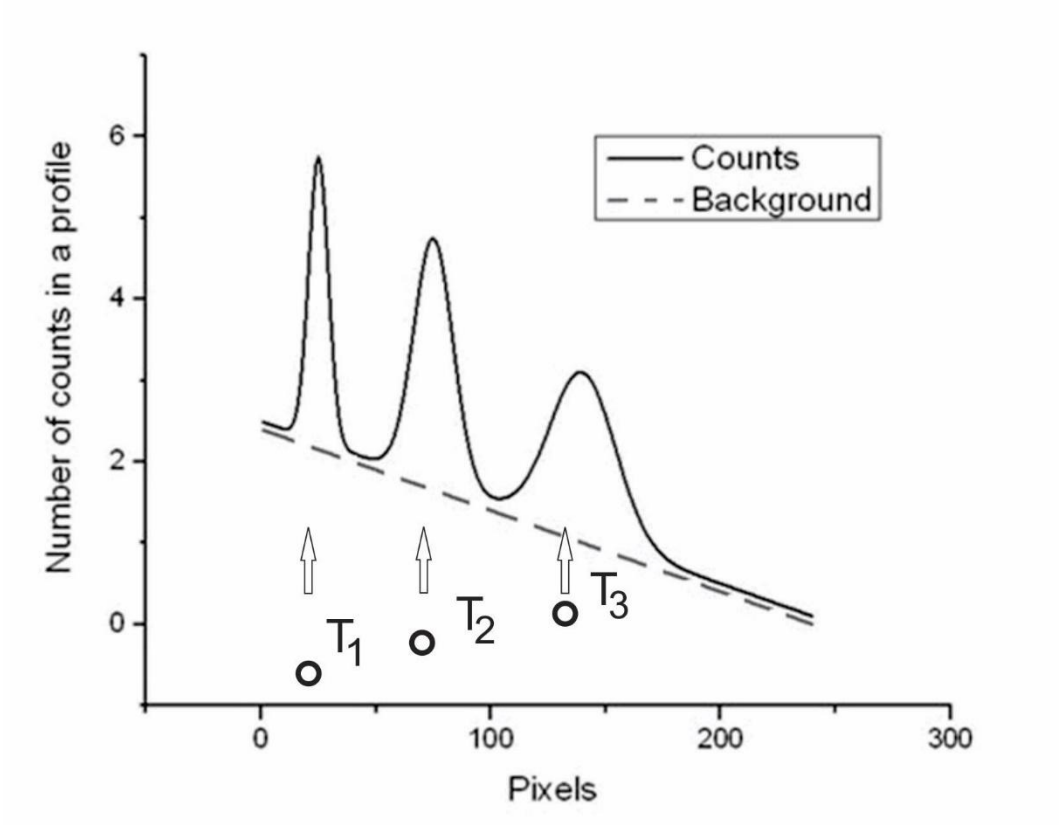

Fig. 4. A sketch of the expected Compton scattering effect on the image profiles of cyclotron-^{99m}Tc-filled capillary tubes at different distances from the gamma camera. The position of the three capillary tubes T_1, T_2, and T_3 is indicated with arrows. The peaks broaden as the Camera-to-object distance increase since the spatial resolution decreases with the distance. However, all peaks are positioned on a decreasing background.

Data acquisition for capillary tubes images with circulating cyclotron-produced technetium TC-TEST_2A sample started 21 hours after EOB and with a duration of 12 hours. A solution containing just an aliquot of it, with activity of 37 MBq, was inserted in the reservoir of the system and images data were collected first with the system in air, and then immersed in water. Similarly, data acquisition (in air and in water) using 45.88 MBq technetium solution from generator (Mallinckrodt pharmaceuticals) was carried out for 13 hours, a few days later. Nine, 10-pixels-thin profiles perpendicular to the capillary tubes were chosen from each image to assess the image background at different points of the field of view (FOV).

The cross section for Compton back-scattering is a complicated nonlinear function of the energy of the gamma rays and it is difficult to determine the individual contribution of each ^{9x}Tc isotope in the image background even if their quantities are *a priori* known. A possible method to check this is to carry out a computer simulation of all processes that take part in the experiment. The simulated Compton-scattering experiment can give an idea about the individual contribution of each technetium nuclide in order to draw conclusions about the image background behavior vs time. Following the idea, the above-described experiment was simulated using GEANT4 toolkit (Agostinelli et al. 2003, Allison et al. 2003). Both the real geometry of the experimental setup described above and the gamma camera parameters were correspondingly modelled. Attention was paid to the size and position of the capillary tubes, the quantity of the immersion liquid, the width of the steel walls of the support and the glass layer of the bottom of the container underneath. A little simplification was applied to the gamma camera collimator configuration with respect to the

original one: instead of the real hexagonal shape of the holes, the simulated ones were assumed to be regular square-shaped, keeping the same basis of 1.7 mm and a septa of 0.2 mm. The simulated gamma-camera sensitive pixels were assumed to have the same width of 0.19 mm as the original ones, but their length was kept equal to the length of the capillary tubes, in order to get directly the integrated number of the counts in the resulting image along the direction parallel to the capillary tubes. The number of gamma rays entered the surface of each pixel was taken into consideration, provided that their energy falls within the narrow acceptance window set during image reconstruction (i.e. between 125 keV and 155 keV).

Simulations with total number of 5×10^8 decay events were carried out separately for each of the isotopes concerned (i.e. ^{99m}Tc, ^{93g}Tc, ^{94g}Tc, ^{95g}Tc, ^{95m}Tc and ^{96}Tc) using the GEANT4 isotopes gamma-ray emission library. The number of the emitted gamma rays from each isotope were scaled to the real isotope abundance taken from gamma-spectrometry analysis. Primary ions of a given technetium isotope were created at a random position, distributed with uniform probability inside the volumes, defined by the three capillary tubes, and then decayed at rest. The gamma rays thus produced were followed until they cross one of the gamma camera pixels (scintillator surface) or until they leave the world volume of the simulation. To reduce the computing time, electrons and neutrinos, produced by the beta decays, were discarded from the simulation stack at the moment of their production. Since GEANT4 simulates by default the complete decay chain until a stable species is achieved, radioactive daughter ions having very long half-life (namely, ^{93}Mo and ^{99g}Tc) were also discarded from the stack, when the process achieved the ground state. For each primary ion, the total number of photons within the aforementioned photopeak energy window that enter each pixel was counted. It was then summed up in a G4THitsMap object, which stores the total number of "good" (i.e. matching criteria) events recorded by each pixel in a given run.

Assessment of cyclotron-^{99m}Tc activity and the activity of ^{9x}Tc isotopes using dose calibrator measurements

An operative procedure was tested to check up the feasibility for a fast and relatively easy assessment of the quality of the produced cyclotron-^{99m}Tc batch. The procedure is based upon the method developed by (Tanguay et al. 2015), concerning the use of commercially-available dose calibrators (DC) to determine the amounts of the ^{9x}Tc impurities in the extracted solution. The gamma-ray activity of the sample is first measured in a dose calibrator placed in a lead shielded container, followed by a second activity measurement of the sample made without lead shielding (in air). In our experiments, we used two different setups in two irradiation tests to measure the gamma-ray activity of the samples. The first one we used is a CRC-15R dose calibrator (Capintec, USA) equipped with a homemade, 5 mm thick, lead shielding while, the second being a dose calibrator VIK 202-5051 (Comecer, Italy), equipped by the manufacturer with a 6 mm thick lead shielding.

The CRC-15R dose calibrator Capintec was used for activity measurements of a 2 ml volume aliquot taken from the TC-TEST_3 sample. Another aliquot, having 1 ml volume, from TC-TEST_4 sample, was measured using a VIK 202-5051 dose calibrator Comecer. The activity measurements of both aliquots were performed at different moments of time, both with and without the lead shielding.

The removable lead shielding used in both measuring devices ensured a significant attenuation effect of the gamma ray component with low energies up to 200 keV (e.g. 200 keV gamma rays intensity is attenuated by a factor of $1/3.6 \times 10^{-3} = 278$ when using 5 mm thickness) including the

ones from ^{99m}Tc. In order to get a proper calibration procedure, activity measurements of a point-like ^{137}Cs calibration source, both in air and with lead shielding were also carried out during all measurements, according to the method described in (Tanguay et al. 2015). Following such an idea, the activity (respectively activity concentration, once known the sample volume) of the samples can be calculated using the readings obtained from the two dose calibrators. However, unlike the one proposed by (Tanguay et al. 2015) a modified formula was applied, without any simplifying assumptions and without the *a priori* known DC calibration factors for ^{9x}Tc impurities, in order either to calculate the ^{99m}Tc activity concentration or to assess the contribution of the remaining ^{9x}Tc contaminant nuclides:

$$A\left(^{99m}Tc\right) = k_1\left(R_{air}(Tc) - k_2 R_{Pb}(Tc)\frac{R_{Pb}\left(^{137}Cs\right)}{R_{air}\left(^{137}Cs\right)}\right), \quad (1)$$

where: $A\left(^{99m}Tc\right)$ is the activity concentration for ^{99m}Tc, determined through gamma spectrometry measurements; $R_{air}(Tc)$ and $R_{Pb}(Tc)$ are the activity readings of the vial in air and with lead shielding respectively; $R_{air}\left(^{137}Cs\right)$ and $R_{Pb}\left(^{137}Cs\right)$ are the corresponding in air and with lead shielding activity readings of ^{137}Cs calibration source. The product $k_1 k_2 R_{Pb}(Tc)\frac{R_{Pb}(^{137}Cs)}{R_{air}(^{137}Cs)}$ in (3) represents the total activity of the other ^{9x}Tc impurities in the sample and can also be used to estimate it once the constants k_1 and k_2 are calculated. When the irradiation conditions (i.e. beam energy, target composition and thickness) are kept unchanged, the calibration constants k_1 and k_2 in (1) are related to the parameters of the measuring systems only: detection geometry (e.g., detector volume, efficiency, thickness of the lead shielding, etc.).

RESULTS

Gamma-spectrometry analysis

The activities of the technetium nuclides in the samples were calculated as a weighted average of the most intense emitted gamma rays from each technetium isotope. Then corrections for the coincidence summing effects in the germanium detectors when cascade transitions in the isotopes were possible have been made. Finally, the obtained activities, calculated back at EOB, are shown in Table 4. The calculated experimental activity uncertainties shown in the table include the uncertainty of the fitted peak areas, the uncertainty in the efficiency calibration where also correction for the summing effects were made, the uncertainty of the sample position and hence the solid angle of the detector and the uncertainty from the coincidence summing effect corrections. For the case of isotope activities calculated from TC-TEST_4B measurements, the error of the fit for the time evolution activity curves has been taken into account as well. It's worth noting that the experimental uncertainties of the activities reported in the table correspond to 1σ confidence level in the peaks fit of the gamma-ray spectra only. They do not include the uncertainties due to other processes, such as the uncertainty of the time lapse to the moment of spectra acquisition and the difference in the geometry, that in general would not introduce a large additional uncertainty of the obtained values. Because of many changing factors (i.e. ^{100}Mo-enriched metallic target mass and thickness, beam energy and spot size, irradiation time, etc.), the absolute activity concentrations of reference samples are difficult to be directly compared. Therefore data are reported as relative

activities of each nuclide with respect to ^{99m}Tc one. As it can be seen from the table, the detection and quantitative measurement of ^{97m}Tc was possible only for the TC-TEST_4B sample due to the higher activity used and the suppression of the 140 keV gamma rays.

Table 4. Radioisotopic composition of cyclotron-produced sodium pertechnetate (rescaled at EOB) for the tests samples (see Tables 1 and 2). The activities of ^{9x}Tc isotopes are normalized to the ^{99m}Tc one.

	Relative Activity (%)			
Nuclide	TC-TEST_1A	TC-TEST_3A	TC-TEST_4A	TC-TEST_4B
^{99m}Tc	1.000E+02	1.000E+02	1.000E+02	1.000E+02
^{93m}Tc	NA	NA	(2.23 ± 0.09)E+00	(2.37 ± 3.24)E+00
^{93g}Tc	(2.12 ± 0.64)E-01	(2.33 ± 0.54)E-02	(5.389 ± 1.12)E-02	(9.075 ± 0.036)E-02
^{94m}Tc	NA	(1.163 ± 0.21)E+00	(6.32 ± 2.0)E-01	(8.18 ± 2.45)E-01
^{94g}Tc	(1.363 ± 0.278)E-01	(1.447 ± 0.15)E-01	(1.66 ± 0.17)E-01	(1.783 ± 0.30)E-01
^{95m}Tc	(3.142 ± 0.64)E-03	(8.69 ± 1.38)E-04	(5.75 ± 0.89)E-04*	(4.490 ± 0.01)E-04
^{95g}Tc	(1.224 ± 0.187)E-01	(1.211 ± 0.19)E-01	(1.130 ± 0.17)E-01	(1.499 ± 0.003)E-01
^{96g}Tc	(1.669 ± 0.246)E-02	(4.252 ± 0.35)E-02	(2.557 ± 0.20)E-02*	(1.500 ± 0.0015)E-02
^{97}Tc	< detection limit	< detection limit	< detection limit	(1.170 ± 0.082)E-03

* Measurement not taken into consideration for the final activity calculations

Taking into account the data collected in Table 4, related to both irradiation beam tests carried out at 15.7 MeV only (see also Table 1), we then obtained the relative activity of all technetium nuclides for future considerations about the radiation absorbed DI calculations. In order to compare properly both datasets, the activities from TC-TEST_3A sample were rescaled to the same irradiation time, as during the irradiation experiment when TC-TEST_4 was prepared. The resulted averaged data values from both experiments at 15.7 MeV are shown in the next Table 5 as relative activities. Here the uncertainties are calculated as a square root of the sum of the squared uncertainties of the corresponding activities (Bevington and Robinson, 2003). Also reported are the Radionuclidic Purity (RNP) limits requested by the recently issued (European Pharmacopoeia, 9.3, 2018) for cyclotron-produced ^{99m}Tc.

Table 5. Relative activities of the technetium nuclides in the extracted solutions from the targets bombarded at 15.7 MeV (rescaled to the EOB time). The data are averaged from TC-TEST_3A, TC-TEST_4A and TC-TEST_4B measurements shown in Table 4. Also shown are the RNP limits for each nuclide reported by the Eu.Parmacopoeia 9.3 which have to be accounted for sodium pertechenetate injection or for the preparation of the pharmaceutical kits at the post EOB injection time.

Nuclide	Activity concentration (%)	RNP (Eu. Pharm. Limits) (%)
^{99m}Tc	(9.659 ± 0.062)E+01	-----

^{93m}Tc	(2.15 ± 0.09)E+00	≤ 1.0E-2
^{93g}Tc	(5.43 ± 1.21)E-02	≤ 4.0E-2
^{94m}Tc	(8.93 ± 3.87)E-01	≤ 2.0E-2
^{94g}Tc	(1.58 ± 0.37)E-01	≤ 4.0E-2
^{95m}Tc	(6.26 ± 1.29)E-04	≤ 5.0E-3
^{95g}Tc	(1.23 ± 0.24)E-01	≤ 7.0E-2
^{96g}Tc	(2.73 ± 0.33)E-02	≤ 7.0E-2
^{97m}Tc	(1.13 ± 0.064)E-03	≤ 1.0E-2

Figure 5 shows the time evolution of all technetium contaminant nuclides' total activity with respect to ^{99m}Tc one obtained after the target irradiation measurements at 15.7 MeV (black curve) The values are obtained using the starting activity taken from Table 5 and the plot time scale is related to events starting from the target EOB. The results may be directly compared and fully confirm the main conclusions about the expected theoretical RNP trend, as reported by (Esposito et al. 2013). For comparison on the same figure in grey color is plotted the correspondent time evolution curve obtained from the irradiation experiment at 19.2 MeV. However, as it was explained above, the contribution of ^{93m}Tc, ^{94m}Tc and ^{97}Tc was not taken into account.

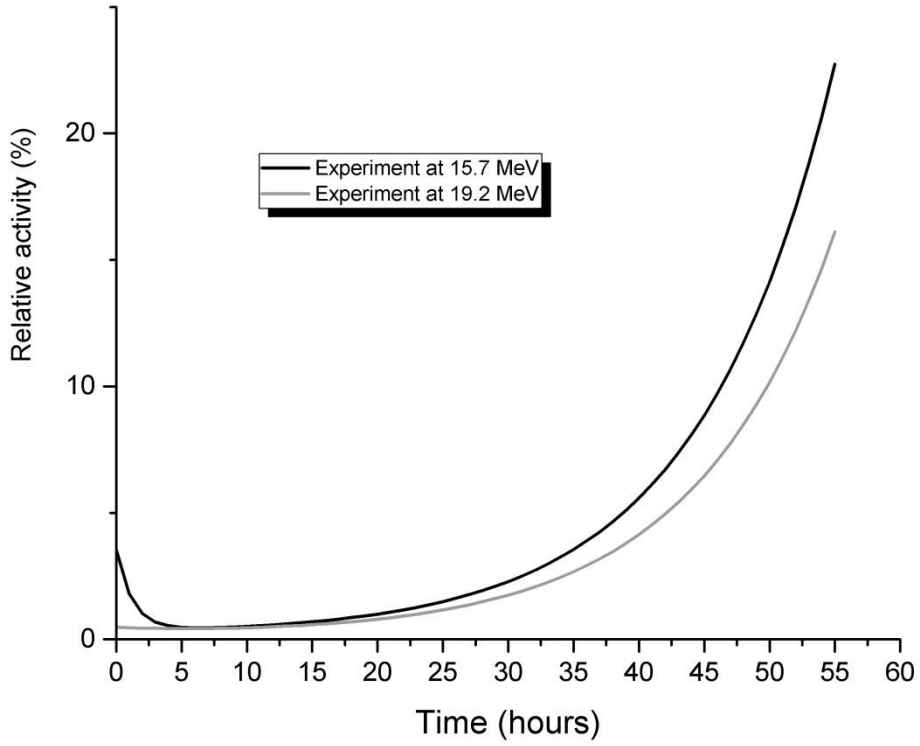

Fig. 5. Time evolution of the total activity of cyclotron- ^{9x}Tc contaminant nuclides relative to ^{99m}Tc activity presenting the target irradiation measurements at 15.7 MeV (black curve) and at 19.2 MeV (grey curve). Note that the contribution of ^{93m}Tc, ^{94m}Tc and ^{97}Tc was not taken into account in curve activity calculations at 19.2 MeV. The time axis origin is related to the EOB event.

In Figure 6 the post-EOB time evolution of the ratio of relative activities contribution for each ^{9x}Tc impurities with respect to the Eu Pharmacopoeia limits are plotted. Values lower, or at least equal, to 1.0 mean parameters within the limits.

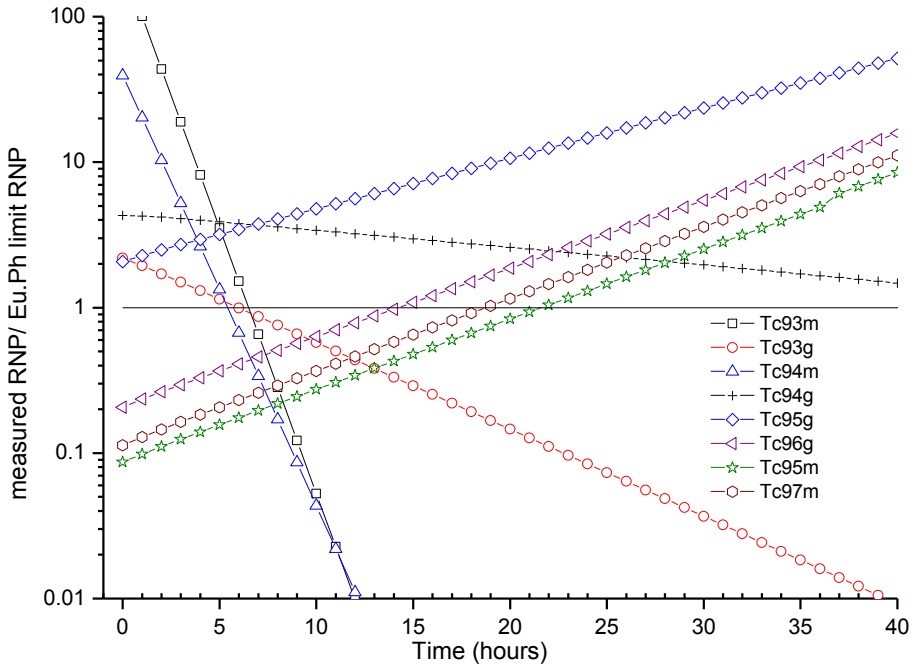

Fig. 6. Post EOB time evolution of the ratio of cyclotron-^{9x}Tc contaminant nuclides relative activities vs. the corresponding European Pharmacopoeia limits.

Quantitative assessment of cyclotron-^{99m}Tc activity through dose calibrator measurements

The post EOB activity concentration time evolution data for TC-TEST_3 samples, measured by the Capintec CRC-15R dose calibrator and calculated using (1) with the optimized coefficients k_1 and k_2, is plotted in Figure 7(a). Similar semi logarithmic plot of the activity concentration as a function of time for TC-TEST_4 samples, measured with the Comecer VIK 202-5051 dose calibrator and the corresponding optimized coefficients k_1 and k_2, is shown in Figure 7(b). For comparison purposes, the corresponding calculated activity concentrations time evolution data, obtained from a single gamma spectrometry measurement of TC-TEST_3A and TC-TEST 4A samples in the beginning, are also shown on both plots. Least squares optimization procedures were carried out, by varying the parameters k_1 and k_2 in order to obtain better correspondence between dose calibrators' measurements and the activity concentration measurements obtained from gamma spectroscopy analysis. It has to be pointed out that both final k values obtained after the optimization procedure (i.e. k_1=1.093 ± 0.02 for Capintec CRC-15R dose calibrator and k_1=0.9371 ± 0.003 for VIK 202-5051), are quite close to 1, thus indicating that both instruments were initially well calibrated for ^{99m}Tc activity measurements.

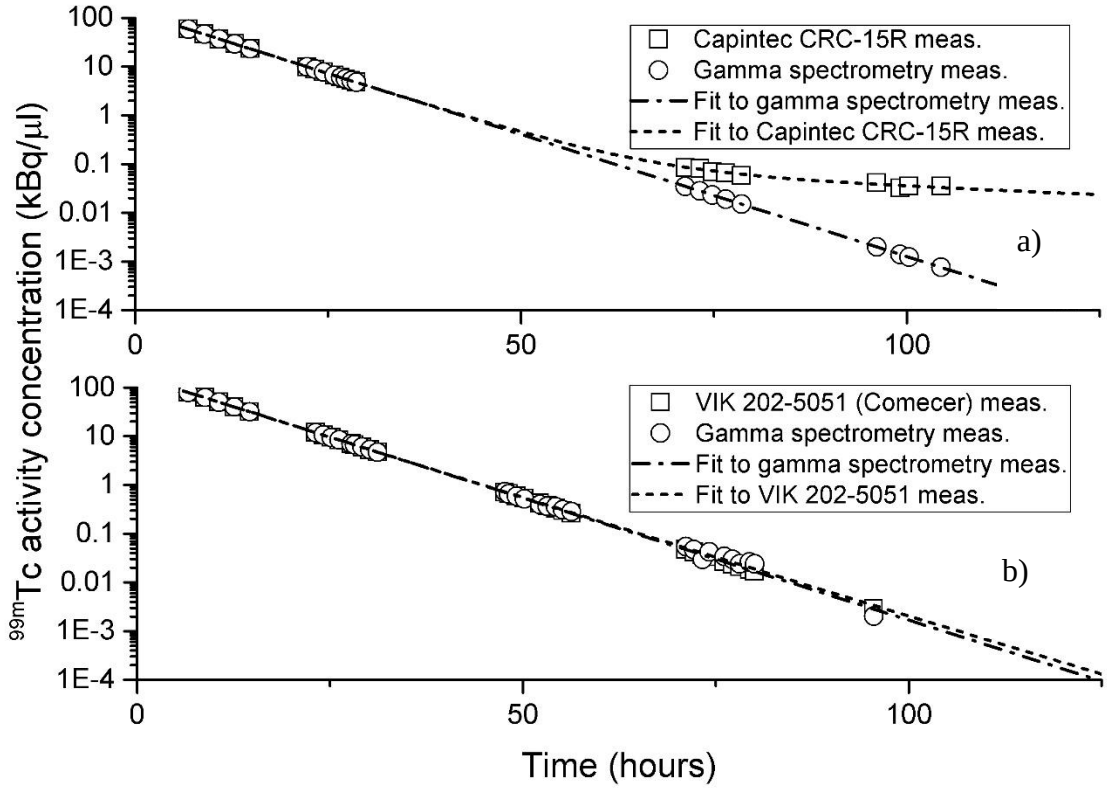

Fig. 7. Cyclotron- ^{99m}Tc activity concentration time evolution post EOB data for: (a) TC-TEST_3 sample using gamma spectrometry measurement data (circle) and rescaled from Capintec CRC-15R dose calibrator measurements with correction factors k_1 = 1.093 ± 0.02 and k_2 = 2.84 ± 0.19 (square); (b) TC-TEST_4 sample using gamma spectrometry measurement data (circle), and rescaled from VIK 202-5051 (Comecer) dose calibrator measurements with correction factors k_1 = 0.9371 ± 0.003 and k_2 = 3.75 ± 0.004 (square).

As eye-guide lines to fit data, the following equation has been used**,** considered that the overall ^{9x}Tc nuclides activity measurement is a linear combination of exponential-driven decay functions:

$$A\left(^{99m}Tc\right) = A_1 exp(-\ln(2)\, t/a_1) + A_2 \exp(-\ln(2)\, t/a_2), \quad (2)$$

where A_1, A_2, a_1, and a_2 are the fitting parameters. Parameters A_1 and a_1 are the activity concentration and the half-life respectively of ^{99m}Tc, being by far the largest contributor component inside the aliquot. The parameters A_2 and a_2 are the activity concentration and the corresponding half-life of a generalized compound consisting of ^{9x}Tc impurities with most intensive higher-energy gamma rays. The obtained values of the fitting parameters for both dose calibrators concerned are shown in Table 6.

Table 6. Fitted parameters of the decay curves for TC-TEST_3 and TC-TEST_4 samples measured using two different dose calibrators.

Fitted parameters of the decay curves

Sample	Dose calibrator	A_1 (kBq/µl)	a_1 (h)	A_2 (kBq/µl)	a_2 (h)
TC TEST3	Capintec CRC-15R	131 ± 0.8	5.96 ± 0.6	0.16 ± 0.02	45.0 ± 0.9
TC TEST4	VIK 202-5051	123.6 ± 0.9	5.75 ± 0.4	49.2 ± 0.2	6.6 ± 0.4

Cyclotron-^{99m}Tc imaging performance assessment

Image data from the dedicated system, filled with a circulating volume of technetium solution from TC-TEST_2A sample (see Table 2), have been acquired with the mini gamma camera. The collected data were used to create two dimensional planar images divided by a time interval of one ^{99m}Tc half-life period (i.e. 6 hours), keeping approximately an equal total number of counts per each image. Once corrected, both for uniformity (NEMA 2001) and photo-peak position (Uzunov et al. 2013), images of 512 × 512 pixels were then obtained (shown in Fig. 8(a) and Fig. 8(b)), by using an energy window centered at 140 keV ± 10 %. The first image, referred to as "Image 1", is related to the acquisition started 8 hrs and 40 min after EOB with a duration of 90 minutes, while the second one ("Image 2") was acquired 14 hrs and 40 min after EOB, for an acquisition time of 180 min. A gamma spectrometry analysis was performed on an aliquot from TC-TEST_2A sample to get a correct determination about the 9xTc isotope abundance during the spatial resolution measurements.

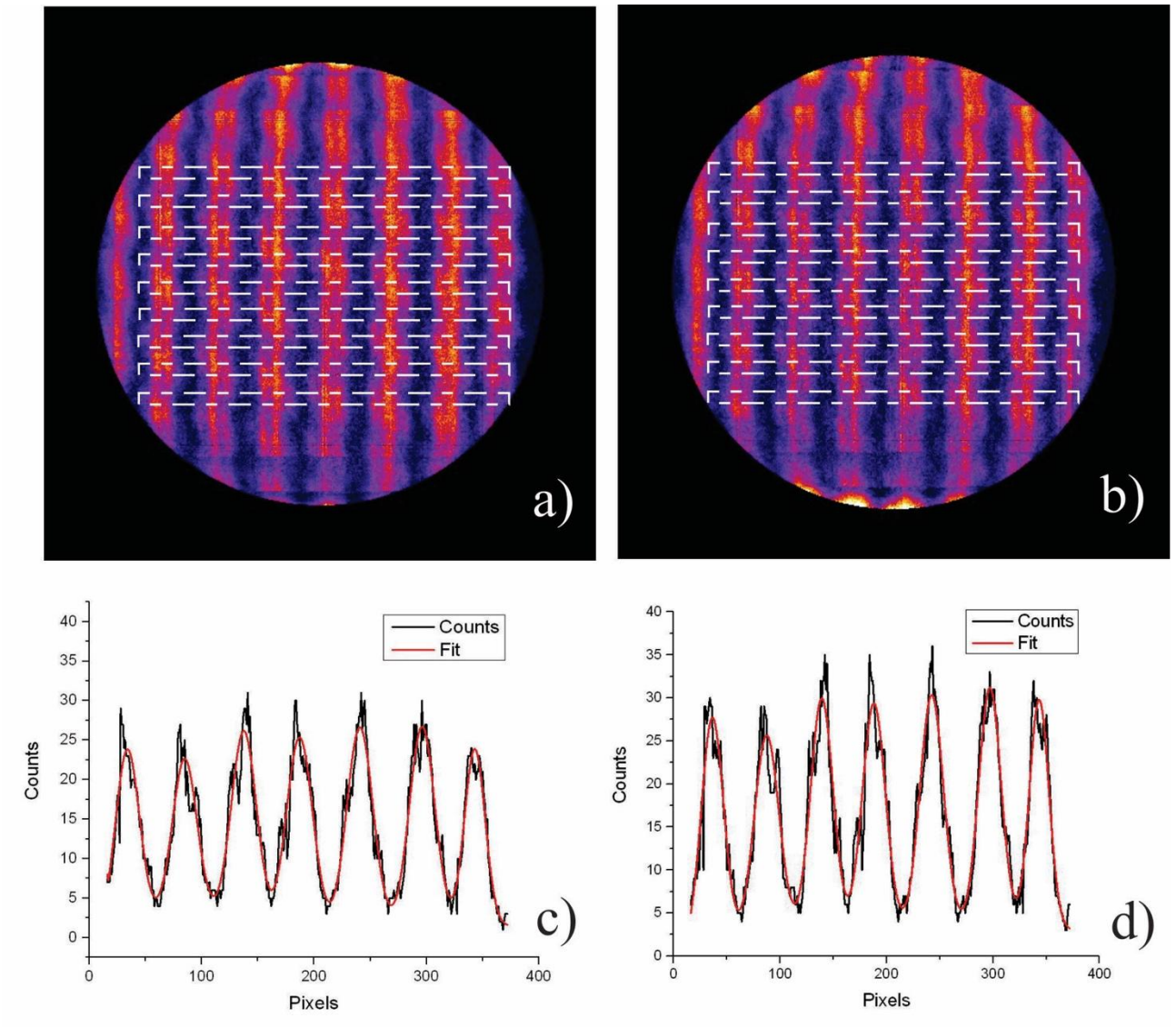

Fig. 8. Images collected from the parallel capillary tubes experimental set-up filled with a circulating solution from cyclotron TC-TEST_2A sample: (a) a reconstruction of Image 1 (8 hrs 40 min after EOB); (b) a reconstruction of Image 2 (14 hrs 40 min after EOB); (c) a profile plot from Image 1 with the corresponding fits; (d) a profile plot from Image 2 with the corresponding fits.

Moreover, aiming to compare the overall spatial resolution performance of images acquired with the gamma camera, using both the cyclotron-Tc and the generator-Tc, we also checked whether the ground state isomer ^{99g}Tc, which is available in larger quantities in the cyclotron-produced ^{99m}Tc solutions (Esposito et al., 2013), could possibly affect the imaging properties. The isotope ^{99g}Tc is present in all technetium solutions and decays to stable ^{99}Ru (half-life of 2.12×10^5 y), emitting beta with 293.5 keV end-point energy. Because of its very long half-life, the concentration of ground-state ^{99g}Tc should not in principle affect the spatial resolution performance of the gamma camera. However, our goal was to check whether it could possibly affect the imaging properties that, to the best of our knowledge, has never been performed before. To meet such an issue, we prepared a set of eluates with different ratios R=N(^{99g}Tc)/N(^{99m}Tc), where N(^{99g}Tc) and N(^{99m}Tc) are concentrations of the ground state and of the metastable isomers respectively. Another reason for the number of samples thus prepared was that we wanted to create a large set (basis) of measurement data for generator-^{99m}Tc eluates. The isomeric ratio R was calculated using the formula:

$$R = N(^{99}Tc)/N(^{99m}Tc) = (1-F)/F \tag{3}$$

Since the daughter nuclide ^{99}Ru is stable, a simplified formula can be applied to the decay chain, with quite a good approximation for the calculation of the factor F in (1), as shown below (Saha 2010):

$$F = \frac{0.87\lambda_1(\exp(-\lambda_1 t) - \exp(-\lambda_2 t))}{(\lambda_2 - \lambda_1)(1 - \exp(-\lambda_1 t))}, \tag{4}$$

where λ_1, λ_2 are the decay constants of ^{99}Mo and ^{99m}Tc respectively and t is the time lapse from the last complete generator elution.

Samples having ratios R equal to 4, 8, 16, 64 and 128 (referred to as R4, R8, R16, R64 and R128 respectively) have been obtained from a commercially available generator, produced by Mallinckrodt Italia, S.p.A. All the eluted solutions were prepared 24 hours after the first full generator elution. According to (3) the starting N(^{99g}Tc)/N(^{99m}Tc) ratio of a generator fresh eluate is equal to 2.554. The first three ratios (R = 4, 8 and 16) were obtained waiting for an additional time lapse equal to 2 h 54min, 7 h 59 min and 13 h 30 min respectively. Samples having even larger ratios R were instead prepared by simply adding an aliquot from a certified standard ^{99g}Tc source for calibration purposes (Eckert & Ziegler Reference & Calibration Sources, code 7099 "Technetium-99 Ammonium pertechnetate in H2O, Calibrated", Solution uncertainty +/-3–5%).

Images from generator-eluted solutions at increasing isomeric ratios R4, R8, R16, R64 and R128 were obtained using the same system of parallel capillary tubes, filled consequently with the different technetium solutions. The camera-to-capillary tubes' distance and the position of the capillary tubes in the field of view have been kept unchanged as during the measurement with TC-TEST_2A.

Table 7 shows the activity concentrations of the major ^{9x}Tc contributors in the sample TC-TEST_2A, as well as the relative activity with respect to the ^{99m}Tc activity, corresponding to the times of the first and the second image acquisition (Image 1 and Image 2). The images' spatial resolution at different positions of the FOV was determined selecting nine 10-pixels large cross-cutting profiles, covering thus the whole FOV area, as shown in Fig. 8(a) and Fig. 8(b). Exploiting the method described in (Uzunov et al. 2004, Uzunov et al. 2005), the FWHM spatial resolution in the camera FOV was then calculated at each peak position (i.e. corresponding to the capillary tube position in the image) for each profile (Fig. 8(c) and Fig. 8(d). The same procedure to determine the FWHM spatial resolution of the mini gamma camera has been applied to the obtained images of generator-^{99m}Tc at increasing isomer ratios R. The FWHM gamma camera spatial resolutions, calculated from Image 1 and Image 2 as well as the corresponding camera spatial resolution calculated from generator-^{99m}Tc at increasing isomer ratios R, are shown in Table 8. The overall averaged FWHM spatial resolution for the gamma camera, related to all measurements performed is shown in the last row.

Table 7. Cyclotron-^{99m}Tc radionuclide composition detected for TC TEST_2A sample, during the imaging spatial resolution measurements.

Imaging spatial resolution measurement time	Nuclide	Measured activity (Bq/μl)	^{99m}Tc relative activity (%)
8 hrs, 40 min after EOB	^{99m}Tc	24152 ± 1640	100
	^{96}Tc	9 ± 1	0.04 ± 0.01
	^{95m}Tc	0.42 ± 0.06	0.0017 ± 0.0003
	^{95g}Tc	62 ± 10	0.26 ± 0.04
	^{94g}Tc	27 ± 8	0.11 ± 0.03
	^{93g}Tc	25 ± 7	0.10 ± 0.03
14 hrs, 40 min after EOB	^{99m}Tc	12084 ± 840	100
	^{96}Tc	8 ± 1	0.07 ± 0.01
	^{95m}Tc	0.42 ± 0.06	0.0034 ± 0.0005
	^{95g}Tc	50 ± 8	0.42 ± 0.07
	^{94g}Tc	11 ± 3	0.09 ± 0.03
	^{93g}Tc	6 ± 2	0.05 ± 0.01

Table 8. Gamma camera FWHM spatial resolution and average values calculated from the capillary tubes images at nine profiles. Both generator-Tc solutions at different isomeric ratios R and cyclotron-^{99m}Tc ones (Image 1 and Image 2) are presented.

Gamma camera FWHM spatial resolution for each profile and overall averaged values(mm)							
Profile	R = 4	R = 8	R = 16	R = 64	R = 128	Image 1	Image 2
1	1.76 ± 0.23	1.80 ± 0.22	1.76 ± 0.20	1.77 ± 0.30	1.80 ± 0.24	2.00 ± 0.25	1.87 ± 0.20
2	1.81 ± 0.17	1.83 ± 0.16	1.84 ± 0.19	1.79 ± 0.18	1.79 ± 0.19	1.88 ± 0.12	1.85 ± 0.16
3	1.81 ± 0.19	1.84 ± 0.19	1.82 ± 0.21	1.87 ± 0.15	1.85 ± 0.14	1.97 ± 0.17	1.84 ± 0.16
4	1.72 ± 0.17	1.67 ± 0.19	1.69 ± 0.22	1.56 ± 0.18	1.64 ± 0.18	1.91 ±0.17	1.85 ± 0.16
5	1.82 ± 0.15	1.85 ± 0.17	1.85 ± 0.15	1.88 ± 0.14	1.87 ± 0.14	1.96 ± 0.16	1.91 ± 0.17
6	1.79 ± 0.13	1.85 ± 0.15	1.80 ± 0.15	1.80 ± 0.19	1.83 ± 0.19	1.98 ± 0.17	1.93 ± 0.20
7	1.82 ± 0.15	1.85 ± 0.14	1.86 ± 0.18	1.83 ± 0.15	1.85 ± 0.16	1.89 ± 0.10	1.82 ± 0.09
8	1.75 ± 0.13	1.77 ± 0.14	1.77 ± 0.18	1.67 ± 0.16	1.67 ± 0.12	1.94 ± 0.18	1.86 ± 0.20
9	1.82 ± 0.17	1.72 ± 0.121	1.80 ± 0.21	1.74 ± 0.15	1.78 ± 0.22	1.84 ± 0.14	1.74 ± 0.24
average	**1.79 ± 0.16**	**1.80 ± 0.17**	**1.80 ± 0.18**	**1.77 ± 0.20**	**1.79 ± 0.18**	**1.93 ± 0.16**	**1.85 ± 0.18**

Influence of higher-energy gamma-ray emitters on imaging background

Typical profiles obtained from collected images in water for both cyclotron-^{99m}Tc and generator-^{99m}Tc are shown in Figure 9 and Figure 10 respectively. Averaged background parameters fits, resulting from all images' profiles, collected both in air and in water, were calculated. The averaged linear background fits from the images of cyclotron-produced technetium, collected in air and in water, are shown with black lines in Figure 11. The corresponding averaged linear background fits from the images of generator-produced technetium are plotted in grey lines. The images acquisition times were set to 60 minutes. In order to keep comparable the background behavior graphs, corrections were applied to both plots, normalizing each background parameters to an equal starting (before the acquisition) count-rate values. Additional corrections were performed, either for the total number of counts registered by the camera, or for decay of the relative activity contribution of contaminant nuclides versus the ^{99m}Tc.

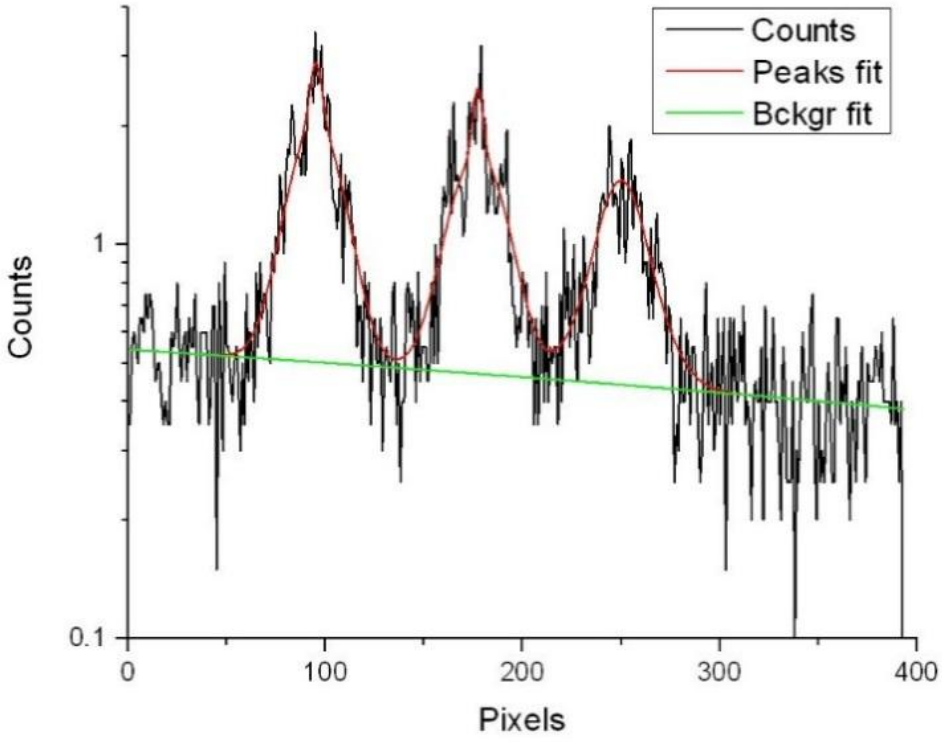

Fig. 9. Profile plot of the immersed in water three-capillary-tubes setup with circulating cyclotron-produced technetium solution TC-TEST_2A. Adapted from "A Study on the Gamma-Ray Background of the Images Obtained Using Accelerator-Produced ^{99m}Tc" by Uzunov et al., 2015, LNL Annual Report, p. 152. Copyright 2015 by the LNL Annual Report. Adapted with permission.

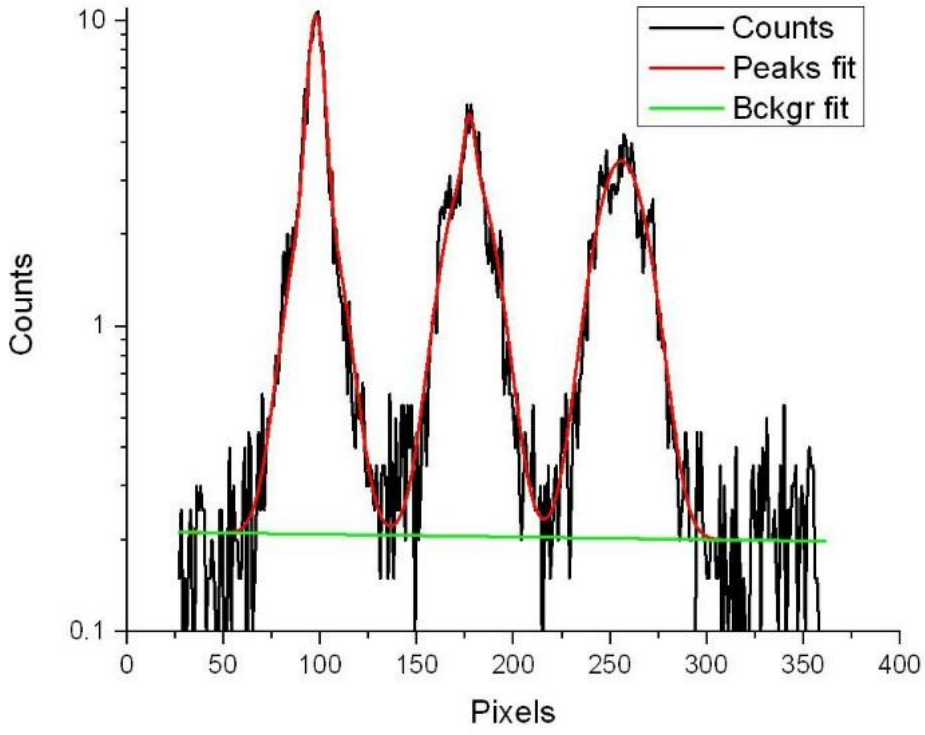

Fig 10. Profile plot of the immersed in water three-capillary-tubes setup with circulating generator-technetium eluate.

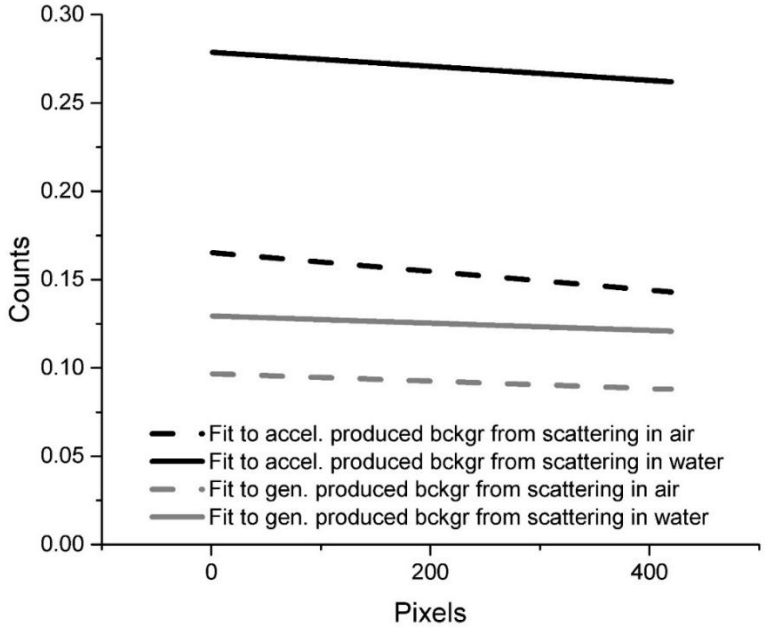

Fig. 11. Plots of the average background fit of images data from the three-capillary-tubes setup, with circulating cyclotron-produced technetium solution TC TEST2_A, collected both in air and in water (black lines). Plots of the average background fit of images from the same setup, but with circulating generator-eluted technetium, collected both in air and in water (grey lines). Adapted from "A Study on the Gamma-Ray Background of the Images Obtained Using Accelerator-Produced 99mTc" by Uzunov et al., 2015, LNL Annual Report, p. 152. Copyright 2015 by the LNL Annual Report. Adapted with permission.

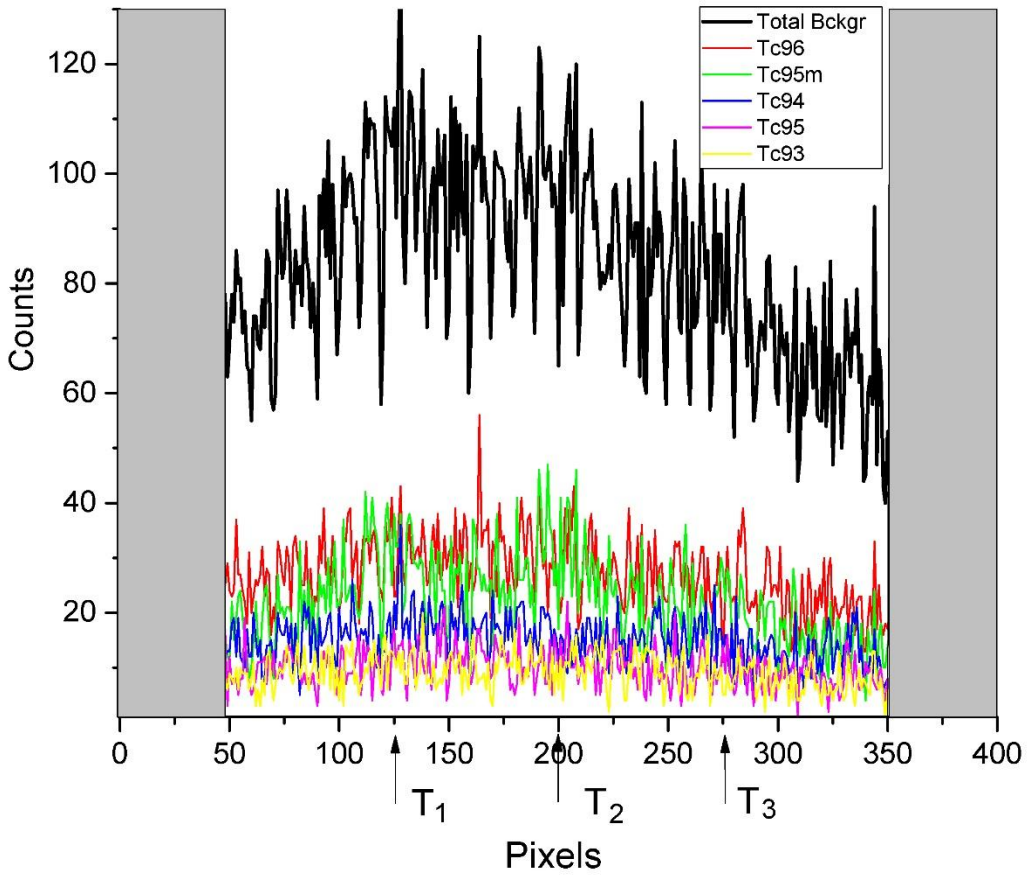

Fig. 12. Simulated profile image of each individual background contribution of technetium nuclides ^{93g}Tc, ^{94g}Tc, ^{95g}Tc, ^{95m}Tc and ^{96g}Tc, and the sum of all isotopes indicated as Total Bckgr. The position of the three capillary tubes T_1, T_2, and T_3 is indicated with arrows. Adapted from "GEANT4 Simulation of the Gamma-Ray Background in the Images Obtained Using Accelerator-Produced ^{99m}Tc" by Selva et al., 2016, LNL Annual Report, p. 156. Copyright 2016 by the LNL Annual Report. Adapted with permission.

Figure 12 shows the GEANT4 simulated cumulative profile image of the sum of all contaminant technetium nuclides ^{93g}Tc, ^{94g}Tc, ^{95g}Tc, ^{95m}Tc and ^{96g}Tc (indicated as "Total Bckgr") , scaled to the corresponding isotope relative activities and calculated for 21 hours after target irradiation, when the real measurement experiment was performed. The walls of the container are indicated in the figure with grey color. The region near the positions of the capillary tubes exhibit a decreasing background similar to the one observed in Figure 4 . The simulated background contribution expected by each nuclide (i.e. ^{93g}Tc, ^{94g}Tc, ^{95g}Tc, ^{95m}Tc and ^{96g}Tc) is presented in color on the same figure. From the plot analysis it may be concluded that the greatest part of the background contribution, 21 hours after irradiation, is due to the Compton scattered gamma-rays emitted by the isotopes ^{95m}Tc and ^{96g}Tc, and, to a slightly lesser extent, from ^{94g}Tc.

DISCUSSION AND CONCLUSION

As expected by the theoretical analyses (Celler et. al 2011, Esposito et al. 2013), ^{9x}Tc contaminant nuclides (Table 3), a result from the direct proton bombardment of ^{100}Mo-enriched molybdenum metallic targets, came into sight in the cyclotron-^{99m}Tc pertechnetate solutions. Such a contribution from other gamma and beta particles, in the overall decay spectrum, turns out to influence the quality of the final gamma-ray images. Our results demonstrate that the image background depends on: (i) the Compton scattering in the media, (ii) the presence of the higher-energy gamma ray emitters in the solution, as well as (iii) the transmission of the gamma rays through the septa of the camera collimator. In this respect, the efforts aiming at improving the imaging performance of ^{99m}Tc are essential in view of a possible, future, cyclotron-based homeland routine production and final use.

A comparison among the relative activities of cyclotron-^{9x}Tc contaminant nuclides from the irradiation experiments carried out both at 19.2 MeV and 15.7 MeV (Table 2) has been performed using a slightly downgraded but still highly ^{100}Mo-enriched molybdenum target material (99.05%).. The results clearly point out that, after the chemical dissolution/purification time necessary to obtain the final cyclotron-^{99m}Tc pertechnetate solution, the total activities of the contaminant nuclides relative to ^{99m}Tc are comparable. Indeed, the relative activities for ^{94g}Tc ($t_{1/2}$=4.88 h), ^{95g}Tc ($t_{1/2}$=20 h) and ^{96g}Tc ($t_{1/2}$=102.72 h) do not differ within the experimental uncertainties.

Concerning the gamma spectrometry analyses a difference is observed for the measured activity concentrations of shorter-half-life nuclide ^{93m}Tc (0.717 hr) and ^{94m}Tc (0.867 hr), in TC-TEST_3A, TC-TEST_4A and TC-TEST_4B. However, one has to keep in mind the time passed from the target irradiation to the spectra acquisition, leading to a larger uncertainty when the measured activity data are extrapolated back to EOB. Some differences between ^{93g}Tc nuclides activities measured in TC-TEST_4A/4B samples have also been observed, although coming from the same TC-TEST-4 source. Our analysis of the measurement conditions conducted later revealed that the differences in the activity values of ^{95m}Tc and ^{96g}Tc from TC-TEST_4A are most probably due to the inaccurate sample positioning during the third spectra acquisition and the corresponding values were therefore not taken into consideration. The other differences are most likely due to the difference in the geometry and the different efficiency calibration procedure used in TC-TEST_4B, being the measurements provided by a different group.

However, due to the aforementioned target processing time requested, ^{94m}Tc, as well as the other short half-life nuclide ^{93m}Tc is not expected to affect the imaging properties. More significant difference is observed between the measured relative activities of ^{93g}Tc ($t_{1/2}$=2.75 h) and ^{95m}Tc ($t_{1/2}$=1464 h) at both proton beam energies. This complies with the theoretical prediction/request concerning the use of lower energy proton cyclotrons (i.e. not exceeding 18-20 MeV, depending upon the target material enrichment level) as by far the optimal solution. Moreover, the experimental cumulative relative activity of technetium contaminant nuclides as a function of time, shown in Figure 5, clearly indicates that a minimum is achieved about 7 hours after EOB and remains within 1% in a time range from 3 up to 20 hours after EOB, which is in accordance with (Esposito et al, 2013).

Concerning the tests performed on the quantitative assessment of cyclotron-^{99m}Tc activity through dose calibrator measurements, a large deviation from the ^{99m}Tc decay line plot from Capintec dose calibrator may be seen in Figure 7(a), for larger times (i.e. >100 hrs). This is most probably due to the thinner lead shielding because of the limited space in the dose calibrator detector head. The later resulted to incomplete shielding effect of the low-energy gamma rays from technetium nuclides having larger half-lives for instance ^{95g}Tc. Such an effect is instead not seen in Figure 7(b), where

the deviation remains within a factor 2 up to ~200 hrs post EOB when using the Comecer VIK 202-5051 dose calibrator. However, one can conclude that the activity concentrations measurements using both dose calibrators, and hence the modified procedure we reported, demonstrate a very good agreement with the gamma spectrometry data. This fact allows us to determine, in a simple and fast way, the quality of produced cyclotron-^{99m}Tc batch. The relative deviation of the measured values remain below 10% even for measurements carried out 48 hours after EOB.

To check whether the ground-state isomer ^{99g}Tc, that present in cyclotron-Tc, can possibly affect the imaging properties of the solution, a series of imaging tests performed with a mini gamma camera Mammocam 1000 were carried out. Spatial resolution of images of a system of parallel capillary tubes with circulating generator-eluted solutions at increasing isomeric ratios R4, R8, R16, R64 and R128 were studied (see Table 8). Spatial resolution data for all layers (column data corresponding to R4, R8, R16, R64 and R128 in Table 8) underwent a single factor ANOVA analysis (Howel 2002, Montgomery 2001) aimed at assessing statistically significant differences between the mean values of unrelated measurements datasets, The analysis did not reveal a considerable difference at the 5% significant level (F-factor = 0.27, while F_{crit}=2.61) for these samples, which rejects the assumption about the possible impact of the ground-state ^{99g}Tc emission on the images' spatial resolution. Such a result is, of course, not surprising since the activity of ground technetium is >10^9 times lower than that of ^{99m}Tc (i.e. $T_{1/2}(^{99m}Tc)/T_{1/2}(^{99g}Tc)$ ~ 3.3E-9) and one should not expect image property deterioration due to the presence of ^{99g}Tc even for quite larger isomeric ratios. However, the conclusion from the ANOVA analyses gives us the strong and objective evidence that such a system of measured values can be used as a basis for further comparison..

On the other hand, the image spatial resolution test on the same system of capillary tubes at the same experimental geometry but using cyclotron-^{99m}Tc solutions demonstrated that a slight degradation (around 7%) of FWHM spatial resolution performance was observed about 9 hours after the EOB. A single-factor ANOVA analysis has been carried out on the aforementioned spatial resolution values from the generator-Tc (column data corresponding to R4, R8, R16, R64 and R128 in Table 8), but with the addition of data from cyclotron-Tc samples (i.e. Image 1, seventh column Table 8). In such a case, the results clearly demonstrated that the cyclotron-^{99m}Tc spatial resolution is somewhat different from the generator-^{99m}Tc ones at the 5% significance level (F-factor = 6.45, while F_{crit}=2.43). Quite similar results have also been observed in the study performed by (Hou et al, 2016(2)), although a different approach has been followed both in the experimental setup and in the Monte Carlo simulations performed. What is interesting however, is the fact that in our measurements the cyclotron-^{99m}Tc spatial resolution improves with time passing and returns within the values typical to the generator-Tc ones about 12 to 14 hours after EOB, while such a behavior has not been observed in the aforementioned work. As a matter of fact, the single-factor ANOVA analysis conducted on the same generator-^{99m}Tc spatial resolution data, but including the FWHM spatial resolution ones from Image 2 in Table 8, taken 6 hours later (i.e. a time lapse equal to one half-life of ^{99m}Tc), do not show difference at the 5% significance level (F-factor = 1.55, while F_{crit}=2.41). The spatial resolution performance of the gamma camera is basically influenced by the fast activity decrease of ^{93g}Tc and ^{94g}Tc, since these are the only nuclides whose relative activity drops down versus the time, according the data in Table 7 and Figure 7.

The larger background level recorded in the scattering experiment images, taken with cyclotron-produced technetium, is due to the presence of nuclides emitting high gamma-ray energies in the solution. This results in a slightly larger slope of the background with respect to the images with the generator-produced one in our experiment, evidencing that such a phenomenon is strictly related to

the ^{9x}Tc contaminant nuclides' relative activity. As it has been confirmed by GEANT4 simulations, the majority in the background contribution is due to the backward Compton scattered gamma rays from ^{95m}Tc and ^{96g}Tc and to a lesser extent from ^{94g}Tc. Therefore, taking into account their long half-lives, it may be pointed out that the influence of these isotopes on the image background would be more significant 25 hours beyond the EOB. Comparing results of present work with the ones reported in a quite similar study by (Hou et al, 2016(2)), it may be argued that a good matching is observed, although the theoretical data as well as the experimental results are somewhat different. Similar conclusions may also be drawn about the influence of proton beam energy on the final image quality: better resolution (i.e. FWHM and background noise) are related to cyclotron-^{99m}Tc produced at energies lower than 20 MeV, and imaging time within 24hrs after EOB, thus basically confirming our theoretical conclusion (Esposito et al. 2013). However, what follows from the simulations (as well as from the real measurements) is that even in the worst experimental condition (the background around the capillary tube in the deepest position), the maximum overall contribution from background noise may be estimated as being 3 – 5%.

In the end it may be concluded that using the direct ^{100}Mo(p,2n)^{99m}Tc reaction route and even making use of slightly downgraded ^{100}Mo-enriched (i.e. 99.05 %) molybdenum target material, a quite high radionuclidic purity level of cyclotron-^{99m}Tc, can be produced, provided that the proton beam energy is kept in the range 15.7– 19.4 MeV. The resulting gamma-ray imaging properties revealed by the final cyclotron-produced pertechnetate product, are indeed well comparable to the standard generator-eluted ones and are basically in compliance with the limits recently issued by the European Pharmacopoeia (European Pharmacopoeia, 9.3, 2018), with respect to either the Radiochemical Purity (RCP) limits, or the Radionuclidic Purity (RNP), as it was also reported in the paper by (Martini et al., 2016). Looking at the post EOB time evolution of relative activities, as shown in Figure 6 it may be inferred that only two nuclides, ^{94g}Tc and ^{95g}Tc, are outside the corresponding limits requested by the European Pharmacopoeia in a time span between 6 and 15 hours post EOB. The relative activities ratios of these nuclides are however within a factor 3 and 7 in the highlighted period. This fact suggests, along with previous considerations, that the best time for patient injection of cyclotron-^{99m}Tc and the subsequent SPECT imaging procedures should occur in this time window, with minimum effects for the final image quality with respect to the generator-Tc, as already emphasized above.

Our next step is to evaluate the effect of the radiation Dose Increase (DI) during the patient diagnostic procedures, based upon the use of some pharmaceutical products, labelled by cyclotron-produced ^{99m}Tc, in order to draw a complete conclusion about its possible future routine applications in nuclear medicine.

Acknowledgments

Full financial support for this work within the scope of the research projects APOTEMA and TECHN-OSP (CSN5) has been provided by the Italian National Institute of Nuclear Physics (INFN). This study was also included in the Coordinated Research Project (CRP-F22062) promoted by the International Atomic Energy Agency (IAEA) 2011–2015, and support by the Agency for attending the various project meetings is gratefully acknowledged. One of the authors (N. Uzunov) would like to acknowledge the support received from the Abdus Salam International Center for Theoretical Physics Trieste, Italy and in particular the Program for Training and Research in Italian Laboratories (TRIL).

References

Agostinelli S. et al. 2003, Geant4, a simulation toolkit, Nucl. Instrum. Meth. A 506 (2003), 250-303

Allison J. et al. 2006, Geant4 Developments and Applications, IEEE Trans. Nucl. Sci. 53(1), 270-278.

Arano Y., 2002. "Recent advances in Tc-99m radio pharmaceuticals". Annals of Nuclear Medicine, 16(2), 79-93.

Basu S. K., Mukherjee G., Sonzogni A. A., 2010, Nuclear Data Sheets for A=95, Nucl. Data Sheets 111(10-11) (210), 2555-2737

Banerjee S., Pillai M.R.A., Ramamoorthy N. 2001. "Evolution of Tc-99m in diagnostic radiopharmaceuticals". Seminars in Nuclear Medicine, 31(4), 260-277.

Banerjee S. R., Maresca K. P., Francesconi L., Valliant J., Babich J. W., Zubieta J. 2005, "New directions in the coordination chemistry of Tc-99m: a reflection on technetium core structures and a strategy for new chelate design". Nuclear Medicine and Biology, 32(1), 1-20.

Bénard, F., Buckley, K. R., Ruth, T. J., Zeisler, S. K., Klug, J., Hanemaayer, V., et al., 2014. Implementation of multi-curie production of 99mTc by conventional medical cyclotrons. Journal of Nuclear Medicine. 55, 1017−1022.

Bevington P. R., Robinson D. K., Data reduction and error analysis for the physical sciences, Third Edition 2003, McGraw-Hill Higher Education

Boschi A., Cazzola E., Uccelli L., et al. 2012, Rhenium(V) and technetium(V) nitride complexes with mixed tridentate π-donor and monodentate π-acceptor ligands. Inorg Chem., 51, 3130-3137

Boschi A., Uccelli L., Pasquali M., et al. 2013, Mixed tridentate π-donor and monodentate π-acceptor ligands as chelating systems for rhenium-188 and technetium-99m nitride radiopharmaceuticals. Curr Radiopharm., 6(3), 137-145.

Browne E., Tuli J. K., 2017, Nuclear Data Sheets for A=99, Nuclear Data Sheets 145, 25-340

Celler, A, Hou, X, Bénard, F, Ruth, T, 2011, Theoretical modeling of yields for proton-induced reactions on natural and enriched molybdenum targets. Physics in Medicine and Biolology, 56, 5469−5484.

Dodd B., Dolan T. J., Laraia M., Ritchie I. 2002, Perspectives on research reactor utilization, Physica B 311, 50–55.

Eckelman W. C., 2009, "Unparalleled Contribution of Technetium-99m to Medicine Over 5 Decades". JACC: Cardiovascular Imaging 2 (3), 364–368, doi:10.1016/j.jcmg.2008.12.013.

Esposito J., Vecchi G., Pupillo G., Taibi A., Uccelli L., Boschi A., Gambaccini M. 2013, Evaluation of 99Mo and 99mTc Productions Based on a High-Performance Cyclotron, Science and Technology of Nuclear Installations, V. 2013, 1-14.

European Pharmacopoeia 9.3. Sodium Pertechnetate (99mTc) injection (accelerator produced). 01/2018: 2891,4801−4803(published online at http://online6.edqm.eu/ep903/)

Hou, X., Tanguay, J., Vuckovic, M., Buckley, K., Schaffer, P., Bénard, F., Ruth, T. J., Celler, A., 2016. Imaging study of using radiopharmaceuticals labeled with cyclotron-produced 99mTc. Physics in Medicine and Biolology. 61, 8199−8213

Howell D. 2002. Statistical Methods for Psychology. Wadsworth Eds., Belmont, CA (USA): 324–325

IAEA. 2002, Specialized software utilities for gamma ray spectrometry. Final report of a co-ordinated research project 1996–2000, IAEA-TECDOC-1275, International Atomic Energy Agency, Vienna, Austria.

IAEA. 2013, Non-HEU Production Technologies for Molybdenum-99 and Technetium-99m, IAEA Nuclear Energy Series no. NF-T-5.4, International Atomic Energy Agency, Vienna, Austria.

IAEA. 2017, Cyclotron Based Production of Technetium-99m, IAEA Radioisotopes and Radiopharmaceuticals Reports No. 2, International Atomic Energy Agency, Vienna, Austria.

ISOFLEX Batch. 2012, Certificate of Analyses Mo-100 enriched molybdenum metallic material, (ISOFLEX-USA).

Klein O., Nishina Y. 1929, "Über die Streuung von Strahlung durch freie Elektronen nach der neuen relativistischen Quantendynamik von Dirac". Z. Phys. 52 (1929), (11-12): 853 and 869. Bibcode:1929ZPhy...52..853K. doi:10.1007/BF01366453.

Krijger G. C., Ponsard B., Harfensteller M., Wolterbeek H. T., Nijsen J. W. F. 2013, The necessity of nuclear reactors for targeted radionuclide therapies, Trends in Biotechnology, Vol. 31, No. 7, 390–396.

Lebeda O., Van Lier E. J., Štursa J., Rális J., Zyuzin A. 2012, Assessment of radionuclidic impurities in cyclotron produced 99mTc, Nucl Med Biol, 39, 1286–1291.

Martini P., Boschi A., Uccelli L., Pasquali M., Duatti A., Pupillo G., Di Domenico G., Salvini A., Strada L., Giganti M., Taibi A., Gambaccini M., Prata M., Manenti S., Groppi F., Loriggiola M., Cicoria G., Marengo M., Lucconi G., Bello M., Uzunov N., Esposito J. 2013, Development of an Automatic Separation/Extraction Module for the Accelerator 99mTc Production from 100Mo-Enriched Molybdenum Metal Targets, 2013 LNL Annual Report, 172–173.

Martini P., Boschi A., Cicoria G., Uccelli L., Pasquali M., Duatti A., Pupillo G., Marengo M., Loriggiola M., Esposito J. 2016, A solvent-extraction module for cyclotron production of high-purity technetium-99m, Applied Radiation and Isotopes, Volume 118, 302-307.

Manenti, S, Holzwarth, U, Loriggiola, M, Gini, L, Esposito, J, Groppi, F, et al., 2014. The excitation functions of 100Mo(p,x)99Mo and ^{100}Mo(p,2n)^{99m}Tc. Applied Radiation and Isotopes 94, 344−348.

Montgomery D. C., 2001. Design and Analysis of Experiments (5th ed.), New York: Wiley. ISBN 978-0-471-31649-7.

NEA, 2017, The supply of Medical Radioisotopes, Medical Isotope Supply Review: 99Mo/99mTc Market Demand and Production Capacity Projection 2017-2022, *NEA Nuclear Development Committee* NEA/SEN/HLGMR(2017)2.

NEMA, NEMA Standard Publication NU 1-2001, Performance Measurements of Scintillation Cameras. USA, Rosslyn: National Electrical Manufacturers Association.

Ott R. J., Flower M. A., Babich J. W., Marsden P. K. 1988, The physics of radioisotope imaging, in The physics of medical imaging, Ed. by Webb S., Taylor & Francis, NY

Pupillo, G, Esposito, J, Gambaccini, M, Haddad, F, Michel, N, 2014, Experimental cross section evaluation for innovative ^{99}Mo production via the (α,n) reaction on 96Zr target. Journal of Radioanaltical and Nuclear Chemistry 302, 911–917

Pupillo, G, Esposito, J, Gambaccini, M, Haddad, F, Michel, N, 2015, Accelerator-based production of ^{99}Mo: A comparison between the ^{100}Mo(p,x) and ^{96}Zr(α,n) reactions. Journal of Radioanaltical and Nuclear Chemistry 305, 73–78

Ruth, T., 2009. Accelerating production of medical radioisotopes., Nature, 437, 536−537.

Ruth, T. J., 2014. The medical isotope crisis: how we got here and where we are going. Journal of Nuclear Medicine and Technology, 42, 245−24 8.

Pillai, M. R. A., Dash, A., Knapp, F. F. R. Jr., 2013. Sustained availability of ^{99m} Tc: possible paths forward. Journal of Nuclear Medicine, 54, 313−323.

Saha G. B. 2010, Fundamentals of Nuclear Pharmacy, sixth ed. Springer-Verlag, ISBN 978-1-4419-5860-0.

Selivanova S. V., Lavallée E'., Senta H., Caouette L., Sader J. A., van Lier E. J., Zyuzin A., van Lier J. E., Guérin B., Turcotte E´., Lecomte R. 2015, Radioisotopic Purity of Sodium Pertechnetate 99mTc Produced with a Medium-Energy Cyclotron: Implications for Internal Radiation Dose, Image Quality, and Release Specifications, The Journal of Nuclear Medicine, Vol. 56, No. 10, 1600–1608

Selva A., Uzunov N., Bello M., De Nardo L., Melendez-Alafort L., Abozeid M., Rosato A., Esposito J., GEANT4 Simulation of the Gamma-Ray Background in the Images Obtained Using Accelerator-Produced 99mTc, 2016 INFN-LNL Report 242, 156 – 157

Tanguay J., Hou X., Esquinas P, Vuckovic M., Buckley K., Schaffer P., Bénard F., Ruth T.J., Celler A. 2015, A fast and simple dose-calibrator-based quality control test for the radionuclidic purity of cyclotron-produced (99m)Tc, Phys Med Biol., Nov 7,60(21), 8229-8247.

Uccelli L, Boschi A, Pasquali M, et al. 2013, Influence of the generator in-Growth time on the final radiochemical purity and stability of 99mTc radiopharmaceuticals. Sci Technol Nucl Install.,2013, 1–7.

Uzunov N., Bello M., Boccaccio P., Moschini G., Bollini D., Baldazzi G., de Notaristefani F. 2004, Accurate determination of the imaging properties of a high-spatial-resolution YAP camera, 2004 INFN-LNL Annual Report, 246 – 247.

Uzunov, N., Bello, M., Boccaccio, P., Moschini, G., Baldazzi, G., Bollini, D., de Notaristefani, F., Mazzi, U., Riondato, M., 2005, Performance measurements of a high-spatial-resolution YAP camera, Physics in Medicine and Biology, 50(3):N11-21.

Uzunov N. M., Bello M., Atroshchenko K., Melendez-Alafort L., Moschini G., Di Domenico G., Gambaccini M., Taibi A., Pupillo G., Esposito J. 2013, Characterization of Scintillation Imaging Camera for Evaluation the Imaging Properties of Isotopes Produced in APOTEMA Experiments , 2013 INFN-LNL Report, 239.

Uzunov N, Bello M., Sartori P., De Nardo L., Melendez-Alafort L., Pupillo G., Di Domenico G., Mateva R., Uccelli L., Boschi A., Groppi F., Salvini A., Taibi A., Duatti A., Strada L., Manenti S., Martini P., Loriggiola M., Rosato A., Esposito J., A Study on the Gamma-Ray Background of the Images Obtained Using Accelerator-Produced 99mTc, 2015 INFN-LNL Annual Report, 152 – 153.

Vučina J. L. 2001, Elution efficiency of Mo-99/Tc-99m generators, Facta Universitatis, Series: Physics, Chemistry and Technology, Vol. 2, No 3, 125-130

Xhixha G., Bezzon G. P., Broggini C., Buso G. P., Caciolli A., Callegari I., De Bianchi S., Fiorentini G., Guastaldi E., Kaçeli Xhixha M., Mantovani F., Massa G., Menegazzo R., Mou L.,

Pasquini A., Rossi Alvarez C., Shyti M. 2013 The worldwide NORM production and a fully automated gamma-ray spectrometer for their characterization, Journal of Radioanalytical and Nuclear Chemistry, Volume 295, Issue 1, 445–457.